Non-gonadal PIWI protein, Aubergine, regulates regenerative stem cell proliferation and tumourigenesis in the *Drosophila* adult intestine.

Karen Bellec[1], Lynsey R Carroll[1], Kathryn AF Pennel[1], Yuanliangzi Tian[1], Yachuan Yu[2], Alexander R Cameron[1], Fabiana Herédia[3,4], Alisson M Gontijo[3,4], Joanne Edwards[1], Rippei Hayashi[5,6, ‡], Julia B Cordero[1,2, ‡]

[1]School of Cancer Sciences, Wolfson Wohl Cancer Research Centre, University of Glasgow, Garscube Estate, Switchback Road, Glasgow G61 1QH, UK. [2]CRUK Scotland Institute, Garscube Estate, Switchback Road, Glasgow G61 1BD, UK. [3] iNOVA4Health, Nova Medical School, Faculdade de Ciências Médicas, NMS, FCM, Nova University of Lisbon, Lisbon, Portugal. [4]cE3c - Centre for Ecology, Evolution and Environmental Changes & CHANGE - Global Change and Sustainability Institute, Department of Animal Biology, Faculty of Sciences, University of Lisbon, Lisbon, Portugal. [5]John Curtin School of Medical Research, The Australian National University, Acton, Australian Capital Territory, Australia. [6]The Shine-Dalgarno Centre for RNA Innovation, The Australian National University, Acton, Australian Capital Territory, Australia.

[‡]Authors for correspondence (rippei.hayashi@anu.edu.au, julia.cordero@glasgow.ac.uk).

Abstract

Somatic stem cells are executors of physiological and pathological proliferation of adult self-renewing tissues, such as the intestine. The actions of intestinal stem cells (ISCs) rely on the integration of cell intrinsic and niche-derived signals, which are necessary to achieve a balanced response to the multiple stimuli that constantly challenge tissue homeostasis and organismal health. Disruption of such balance is causative of age-associated tissue dysfunction and hyperproliferative conditions, including inflammation and cancer.

The highly conserved PIWI-interacting RNAs (piRNAs) biosynthesis pathway, also known as the PIWI pathway, has been classically studied in the *Drosophila* germline for its role in the repression of transposable elements (TEs) and the regulation of germline stem cell homeostasis. Recent reports have emerged on a role of Piwi, the founding member of the pathway, in the maintenance of ISC homeostasis in the adult *Drosophila* midgut. The implications of these findings regarding a general role of the PIWI pathway and piRNAs in the intestine remain to be addressed. Here, we characterise a cell autonomous role of the PIWI family protein Aubergine (Aub) in ISCs. We show that, while dispensable for homeostatic self-renewal of the midgut, inducible Aub is essential to regulate ISC proliferation following acute damage of the intestinal epithelium and in oncogenic settings. Our work suggests that the role of Aub in ISCs is independent of its piRNAs regulatory function. Instead, Aub drives ISC proliferation through the regulation of protein synthesis, including induction of regenerative stem cell factors Myc and Sox21a, and a parallel pathway involving the eukaryotic initiation factor 3 complex (eIF3). In summary, our results discover a role for Aub in damage-induced proliferation of the adult *Drosophila* intestine involving the regulation of major regenerative pathways and the protein translation machinery. Furthermore, we present genetically defined hyperplastic settings fostering distinct functions of Aub in intestinal tumourigenesis.

Introduction

Since their discovery as regulators of germ line stem cell self-renewal in the fruit fly *Drosophila melanogaster* (Cox et al., 1998, Lin and Spradling, 1997, Cox et al., 2000), the highly conserved proteins of the PIWI family have been extensively studied for their role in protecting and maintaining genome integrity in animal germline through transcriptional and post-transcriptional silencing of TEs (Siomi et al., 2011, Vagin et al., 2006, Brennecke et al., 2007, Li et al., 2009, Aravin et al., 2007b, Houwing et al., 2007, Aravin et al., 2007a, Saito et al., 2006, Aravin et al., 2006, Girard et al., 2006). Genome defence mechanisms by the PIWI pathway rely on the biogenesis and maturation of piRNAs, a specific type of 24-32 nucleotides long small non-coding RNAs, that bind the PIWI-clade Argonaute proteins hereafter called PIWI proteins. piRNAs are derived from transposon-dense genomic loci called piRNA clusters (Brennecke et al., 2007). After a precursor RNA is transcribed and exported from the nucleus, a set of dedicated RNA helicases and nucleases process it and load the mature piRNA onto a PIWI protein. The PIWI protein loaded with a piRNA exerts gene silencing by cleaving mRNAs or recruiting chromatin modification enzymes to install heterochromatin. In the *Drosophila* germline, PIWI proteins Piwi and Aub mainly bind piRNAs that target TEs in the nucleus and the cytoplasm, respectively (Pane et al., 2007, Nishimasu et al., 2012, Brennecke et al., 2007, Ipsaro et al., 2012), while Argonaute 3 (AGO3) predominantly binds TE sense piRNAs to aid the production of TE antisense piRNAs (Gunawardane et al., 2007, Brennecke et al., 2007, Han et al., 2015, Wang et al., 2015b, Malone et al., 2009, Li et al., 2009).

While in-depth knowledge regarding the composition and molecular function of the PIWI pathway derives primarily from its study in the germline and its role in TEs repression, numerous reports have documented the presence of PIWI proteins in adult somatic tissues and/or roles for these proteins expanding beyond piRNAs and TE regulation (Ross et al., 2014, Pal-Bhadra et al., 2004, Brower-Toland et al., 2007, Huang et al., 2013, Mochizuki et al., 2002, Jones et al., 2016, Sousa-Victor et al., 2017, Tang et al., 2023, Rajasethupathy et al., 2012, Sharma et al., 2001).

Pioneering work in *Drosophila* reported ectopic expression and tumour promoter functions of germline genes, including PIWI pathway components, in a malignant brain tumour model (Janic et al., 2010). Similarly, growing evidence in humans suggests misexpression of PIWI proteins and/or piRNAs in multiple cancers (Qiao et

al., 2002, Shi et al., 2020, Wang et al., 2021, Huang et al., 2021, Wang et al., 2016, Li et al., 2019, Martinez et al., 2015, Lin et al., 2021, Krishnan et al., 2016, Xie et al., 2018, Martinez et al., 2016). However, the link between ectopic PIWI gene expression or piRNAs as well as the identity of piRNAs in cancer remain debatable (Shi et al., 2020, Li et al., 2020, Genzor et al., 2019, Zhang et al., 2013, Liu et al., 2021, Tosar et al., 2021). Similarly, in colorectal cancer (CRC), upregulation of several piRNAs has been correlated with cancer progression, metastasis, and poor overall survival (Yin et al., 2019, Weng et al., 2018). Yet, the functional significance of PIWI proteins and piRNAs in intestinal health and disease remains largely unknown.

Most similar to the mammalian small intestine, the adult *Drosophila* midgut epithelium is maintained and repaired by dedicated stem cells (Micchelli and Perrimon, 2006, Ohlstein and Spradling, 2006) **(Fig. 1A)**. In addition to intestinal stem cells (ISCs), the fly midgut epithelium consists of two subtypes of undifferentiated stem cell progeny, namely, enteroblasts (EBs) and pre-enteroendocrine cells (EEPs), which are precursors of absorptive enterocytes (ECs) and secretory enteroendocrine cells (EEs), respectively (Beehler-Evans and Micchelli, 2015, Zeng and Hou, 2015, Chen et al., 2018) (**Fig.1A'**). Epithelium intrinsic cells, including EBs and ECs, or cells from gut associated tissues, such as the visceral muscle (VM), terminal tracheal cells (TTCs) and enteric neurons (ENs) are components of the intestinal microenvironment, which non-autonomously influence ISC proliferation through paracrine signalling (Perochon et al., 2021, Tamamouna et al., 2021, Petsakou and Perrimon, 2023) (**Fig.1A'**).

Recent work in the adult *Drosophila* midgut has identified a functional role of stem cell expressed Piwi in the maintenance of ISCs during tissue homeostasis (Tang et al., 2023) or following pathogenic and age-associated stress (Sousa-Victor et al., 2017). Whether these observations reflect on a general role of the PIWI pathway and piRNAs in the adult intestine remain to be addressed. In our study, we discovered that the PIWI protein Aub is upregulated within the stem/progenitor compartment of the adult midgut in response to intestinal damage or oncogenic stress and it is required to regulate regenerative and hyperplastic ISC proliferation. Despite the presence of a piRNA signature in the midgut and in ISCs/EBs revealed by small RNA sequencing, combined genetic and functional studies indicate that the induction of ISC proliferation by Aub is independent of its canonical piRNAs

regulatory function. Mechanistically, Aub drives regenerative proliferation in the intestine through the regulation of protein synthesis, including induction of stem cell Myc and Sox21a, and activation of a parallel pathway involving the eukaryotic initiation factor 3 complex (eIF3). Interestingly, we identified genetically defined tumour settings revealing distinct roles of Aub in hyperplastic ISC proliferation. Altogether, our results uncover a previously unrecognised role of Aub in physiological and pathological proliferation of the adult *Drosophila* midgut and provide defined platforms for further *in vivo* studies on the role of PIWI proteins and piRNAs in intestinal health and disease.

Results

Aub is required for regenerative proliferation of ISCs following damage to the adult midgut epithelium.

To study the role of the PIWI pathway in the adult *Drosophila* intestine, we first assessed the expression of its core components *piwi*, *aub* and *ago3,* by RT-qPCR in midguts from mated females (**Fig.1A**, **B**). We observed low but detectable levels of *piwi*, *aub* and *ago3* mRNAs in homeostatic midguts with a slight enrichment of *piwi* and *ago3* in the posterior half (R4-R5) of the midgut (**Fig.1A**, **B**), a region that is characterised for its higher degree of ISC proliferation and predominantly studied in intestinal regeneration research (Buchon et al., 2013, Marianes and Spradling, 2013). We next assessed the role of the PIWI pathway in intestinal regeneration by feeding wild type, *piwi*, *aub* or *ago3* whole mutant flies with sucrose or with the pathogen *Pseudomonas entomophila* (*Pe*) to induce intestinal damage (Jiang et al., 2009). We quantified proliferating ISCs in posterior midguts of mated females by staining against the mitotic marker phosphorylated histone H3 (PH3) (**Fig.1C-E**). As expected, *Pe* feeding caused robust ISC proliferation in wild type flies when compared to their sucrose fed counterparts (**Fig.1C, D**). Loss of *piwi* mildly diminished intestinal regeneration in agreement with previously described roles of the protein in homeostatic and post-stress ISC maintenance (Sousa-Victor et al., 2017, Tang et al., 2023) (**Fig.1C, D**).

Interestingly, aub^{HN2}/aub^{QC42} mutant animals showed a significantly greater impairment in midgut regeneration (**Fig.1C, D**). aub^{HN2}/aub^{QC42} trans heterozygotes are the gold standard and best characterised *aub* loss of function mutants, used in most studies where Aub function has been analysed (Malone et al., 2009, Wang et al., 2015b, Rojas-Ríos et al., 2017). These alleles were generated by ethyl methanesulfonate mutagenesis (Schüpbach and Wieschaus, 1991). aub^{HN2} contains a nonsense mutation while aub^{QC42} contains a point mutation, both resulting in a non-functional protein. We also tested other and less characterized loss of function alleles of *aub*, aub^{g1}/aub^{g2} and aub^{clash}, which showed consistent, albeit milder impairment of intestinal regeneration (**Fig.1E**). aub^{g1}/aub^{g2} have been generated using CRISPR/Cas9 and contain a frameshift mutation resulting in an early translational stop. This trans heterozygote combination is considered a molecular null based on morphological phenotypes, protein levels and expression of small

subset of TEs in germline studies (Senti et al., 2015). *aub*^{clash} is a loss of function allele characterised in germline studies based on its effect on germline morphology and female/male fertility (Sahin et al., 2016).

Unexpectedly, whole body loss of *ago3*, an obligate partner of *aub* in the Ping-Pong pathway, or ISCs and EBs (stem/progenitors) gene knockdown by RNAi expressed under the control of the temperature-sensitive *escargot-Gal4, UAS-GFP; tubGal80* (*esg*^{ts}), had no impact on intestinal regeneration upon damage (**Fig.1C, D** and **Fig.S1A**). Importantly, conditional knockdown of *aub* in ISCs/EBs was sufficient to abolish regenerative ISC proliferation (**Fig.1F, G** and **Fig.S1A**). However, unlike *piwi* (Tang et al., 2023), knocking down *aub* did not cause any detectable effects in homeostatic ISC renewal (**Fig.S1B, C**). These data point to a specific role of stem/progenitor cell Aub in regenerative ISC proliferation of the adult *Drosophila* midgut. Consistently, immunostaining experiments confirmed the post-transcriptional upregulation of Aub expression in ISCs/EBs upon midgut damage (**Fig.1H, J, K**), which was markedly reduced by RNAi driven *aub* knockdown in ISCs/EBs (**Fig.1I, J**). Next, to distinguish the cell type where *aub* functions to regulate ISC proliferation, we induced gene knockdown in EBs or ISCs only using cell specific drivers *Su(H)GBE-Gal4,UAS-GFP; tub-Gal80*^{ts} or *esg-Gal4,UAS-GFP; Su(H)GBE-Gal80, tub-Gal80*^{ts}, respectively (hereafter referred to as *EB*^{ts} and *ISC*^{ts}, respectively; **Fig.1L, M**) (ZengChauhan and Hou, 2010, Wang et al., 2014). While no impact on normal intestinal regeneration was observed upon knocking down of *aub* in EBs only (**Fig.1L**), gene knockdown of *aub* in ISCs was sufficient to recapitulate the impairment in regeneration observed in midguts with dual ISCs/EBs *aub* RNAi expression (**Fig.1M**). Collectively, these results demonstrate a cell autonomous role of damage induced Aub in regenerative ISC proliferation in the adult *Drosophila* midgut.

Midgut stem/progenitor cells express TE piRNAs independently of Aub.

Aub and the PIWI pathway have been extensively described for their role in the repression of germline TEs through piRNAs (Brennecke et al., 2007, Gunawardane et al., 2007, Malone et al., 2009, Wang et al., 2015b). However, broader biological functions of Aub have been described and include the regulation of localisation, stability and translation of specific mRNAs in the *Drosophila* germline and in the embryo (Barckmann et al., 2015, Dufourt et al., 2017, Ramat et al., 2020,

Becalska et al., 2011, WilsonConnell and Macdonald, 1996, Cook et al., 2004, Ma et al., 2017, Rojas-Ríos et al., 2017). Such roles of Aub rely on piRNA-dependent (Barckmann et al., 2015, Dufourt et al., 2017, Ramat et al., 2020, Rojas-Ríos et al., 2017, Rouget et al., 2010, Vourekas et al., 2016, Rojas-Ríos et al., 2023) and piRNA-independent mechanisms (Ma et al., 2017). Whether there is involvement of piRNAs in the role of Piwi in the adult *Drosophila* midgut, remains unresolved (Sousa-Victor et al., 2017, Tang et al., 2023).

We took multiple complementary approaches to understand the mechanisms of action of Aub in the adult *Drosophila* midgut. Firstly, we tested whether we could recapitulate the effect of *aub* knockdown on regenerative ISC proliferation by whole body loss and/or adult ISC/EB specific knockdown of additional components of the primary pathway (Armitage (Armi); Rhino (Rhi)) or the Ping-Pong pathway (Vasa; Spindle-E (SpnE)) (**Fig. S1D, E**). As in the case of Ago3 (**Fig. 1C, D** and **Fig. S1A**), we detected no effect on intestinal regeneration upon loss *spnE* (**Fig.S1D).** However, whole body loss or ISC/EB knockdown of the other genes assessed led to a significant decrease in ISC proliferation upon intestinal damage (**Fig.S1D, E**). Given the role of complementary PIWI pathway members regulating each other's stability in the germline (Senti et al., 2015, Wang et al., 2015b), we tested whether *piwi* or *vasa* downregulation within ISCs/EBs might impact Aub stability and therefore explain their effect on ISC proliferation through indirect Aub regulation. However, in neither case did we see a change in the upregulation of Aub in regenerating midguts (**Fig.S1F-I**). These data suggest that *piwi* and *vasa* act independently from Aub in the midgut to regulate intestinal regeneration.

Next, we performed small RNA sequencing of oxidized samples of adult whole midguts from wild type and *aub* mutant flies to assess the overall presence of piRNAs in this tissue (**Fig.S2A**). Importantly, we took advantage of the 2′-*O*-methylation present at the 3′ ends of piRNAs that confers resistance to sodium periodate oxidation (Kirino and Mourelatos, 2007, Ohara et al., 2007, Saito et al., 2007, Houwing et al., 2007). Consequently, RNA samples were enriched with piRNAs versus other, and potentially more abundantly present, small RNAs populations. Although much less prominent than in oxidized libraries from ovaries (**Fig.S3A**), oxidation of gut libraries revealed an enrichment of 23-28 nucleotide long TE antisense small RNAs (**Fig.S2B**). Importantly, those RNAs showed nucleotide biases characteristic of piRNAs: Uridines at the 1st base position of TE antisense

reads (AS), and to a lesser extent Adenines at the 10th base position of TE sense reads (S). Notably, this enrichment was not visible in previously published unoxidized libraries (Siudeja et al., 2021)(**Fig.S3B**), emphasising the importance of library oxidation to observe small enrichments in piRNAs. Interestingly, the abundance of AS piRNAs observed in whole midguts appeared overall diminished in *aub* mutant tissues (**Fig.S2B, B'** versus **Fig.S2C, C'** and **Fig.S2D, E**). While these data may suggest an involvement of Aub in the regulation of piRNAs in the adult midgut, whole midgut samples contain very heterogeneous cell populations, including gut-associated-trachea and visceral muscle, in addition to the multiple cellular subtypes present within the midgut epithelium itself. This cell heterogeneity often underestimates molecular information from cells underrepresented in the midgut and it is insufficient to address cell specific gene function. To better determine if our results in whole adult midguts are reflective of the presence of piRNAs and/or a piRNA regulatory function of Aub in ISCs, we next conducted small RNA sequencing of oxidized libraries from sorted control or *aub-RNAi* expressing ISCs/EBs (**Fig.2A**). Compared to whole midgut samples, small RNA sequencing from ISCs/EBs of control and regenerating midguts showed a stronger piRNA signature (**Fig.2B** versus **Fig.S2B**). However, piRNA abundance in ISCs/EBs was not reduced by cell specific knockdown of *aub* (**Fig.2B, B'** versus **Fig.2C, C'**). If anything, we observed an unexplained trend towards higher piRNA counts in ISCs/EBs from *aub-RNAi* midguts (**Fig.2D, E**).

The tiles analysis of genome-unique piRNA mappers in ISCs/EBs versus those in ovaries showed that piRNA germline-expressed clusters 38C and 42AB are more abundant in ISCs/EBs than those from the somatic cluster flamenco (**Fig.2F**). This is consistent across all conditions and genotypes analysed (**Fig.S3C-F** and **Fig.S3G** for ovaries). In summary, our results suggest that the overall piRNA signature seen in ISCs/EBs from adult midguts is distinct from that observed in the ovaries. However, *aub* downregulation does not impair ISC/EB piRNAs.

Aub regulates intestinal regeneration independently of its piRNA regulatory function.

To further address the role of Aub in the midgut in relation to its piRNA regulatory function, we performed mRNA sequencing from control or Aub-depleted ISCs/EBs to measure the abundance of TE mRNAs in homeostasis (Sucrose) and

upon regeneration (*Pe*) (**Fig.3A, B** and **Fig.S4A, B**). While several TEs, such as *copia*, *roo* and *Doc*, were abundantly expressed in ISCs/EBs in both conditions, this was independent of the presence of Aub (**Fig.3A, B** and **Fig.S4A, B**). However, these TEs are neither abundantly expressed nor under the control of Aub in the ovaries (**Fig.S4C**) (Senti et al., 2015). Interestingly, we observed that *flea* expression, a TE regulated by Aub in the germline (Sienski et al., 2015) (**Fig.S4C**), was also upregulated in ISCs/EBs (**Fig.3A, B** and **Fig.S4A, B**). However, *flea* upregulation was largely associated with the presence of *Pe* infection rather than with Aub expression (**Fig.3A, B** and **Fig.S4A, B**). These data are consistent with recent work suggesting that stress-associated TE regulation in the midgut may be carried out by mechanisms independent of the piRNA machinery (Siudeja et al., 2021). Next, we used site-directed transgenesis to generate fly lines carrying inducible GFP tagged wild type Aub (*UAS-aub*^{WT}) or mutant isoforms (*UAS-aub*^{AA} and *UAS-aub*^{ADH}*,* **Fig.S4D**). *UAS-aub*^{AA} contains a double point mutation in the PAZ domain, responsible for the loading of piRNAs (Barckmann et al., 2015) while *UAS-aub*^{ADH} carries a single mutation in the PIWI domain, responsible for Aub's endonuclease activity and essential for piRNA biogenesis (Wang et al., 2015b). Mutations in *aub* have been previously correlated with female sterility, a reduced size of the ovaries and embryonic lethality (Sahin et al., 2016, Schüpbach and Wieschaus, 1991, Barckmann et al., 2015, Wang et al., 2015b). We first verified the general functionality of our transgenes by assessing their ability to revert female sterility in *aub* mutant flies (**Fig.S4E**). Consistent with previous reports (Wang et al., 2015b) we observed that only *UAS-aub*^{WT} could partially restore fertility when expressed in the germline (**Fig.S4E**). Next, we used *esg-Gal4* to drive expression of the different transgenes in the midgut of wild type flies and used anti-GFP and anti-Aub staining as proxies to measure ISC/EB transgene expression levels and confirmed comparable transgene expression in the midgut (**Fig.3C-E**). Next, we expressed *UAS-aub*^{WT}, *UAS-aub*^{AA} or *UAS-aub*^{ADH} in ISCs/EBs from trans-heterozygote *aub*$^{HN2/QC42}$ flies (Harris and Macdonald, 2001, Schüpbach and Wieschaus, 1991, Schüpbach and Wieschaus, 1989) using *esg-Gal4* (**Fig.3F-H**). Aub expression by the different constructs was significantly increased when compared to *aub*$^{HN2/QC42}$ mutant flies, in both sucrose and *Pe* conditions (**Fig.3F, G**). Despite the slightly reduced Aub levels upon the expression of *UAS-aub*^{ADH} compared to the other transgenes, we observed a significant rescue of regenerative

ISC proliferation in all cases when compared to *aub*$^{HN2/QC42}$ midguts (**Fig.3F-H**). Altogether, our results suggest that Aub is not necessary to repress TEs or induce the piRNA signature of ISCs/EBs and that the piRNA regulatory function of Aub is dispensable for the activation of ISC proliferation in the adult *Drosophila* midgut.

Aub regulates ISC proliferation through the translation of core regenerative factors in the adult midgut.

To further characterize the processes underpinning the role of Aub in the midgut, we next assessed the effect of *aub* knockdown on the activity of signalling pathways essential for the regenerative capacity of the intestinal epithelium. The EGFR/MAPK, Wnt and JAK-STAT pathways require ISC activation of their respective effectors, Sox21a, Myc and Socs36E, to drive intestinal regeneration (Buchon et al., 2010, Biteau and Jasper, 2011, Xu et al., 2011, Jiang et al., 2011, Jiang et al., 2009, LinXu and Xi, 2010, Zhou et al., 2013, LinXu and Xi, 2008, Cordero et al., 2012b). We hypothesized that these transcription factors would represent good candidates to mediate the exclusive cell autonomous function of Aub within ISCs (**Fig.1L, M)**. In the first instance, we performed RT-qPCR analysis of homeostatic and regenerating control and *aub* knockdown midguts, which showed no effect of Aub on the upregulation of *sox21*a (**Fig.S5A**), *myc* (**Fig.S5B**) or *socs 36e* mRNA (**Fig.S5C**) in *Pe* treated midguts.

Well documented biological functions of Aub in the germline and embryo include control of the translation of mRNAs coding for specific proteins, including transcription factors (WilsonConnell and Macdonald, 1996, Harris and Macdonald, 2001, Ma et al., 2017, Ramat et al., 2020, Rojas-Ríos et al., 2017). Protein synthesis is necessary for the adaptive proliferative response of ISCs to changes in diet and nutrient availability (Obata et al., 2018, Bonfini et al., 2021). Protein translation, measured by puromycin incorporation (Bonfini et al., 2021, David et al., 2012, DeliuGhosh and Grewal, 2017), was significantly increased in ISCs of regenerating midguts (**Fig.4A, C**), and this was dependent on *aub* expression (**Fig.4B, C**). We therefore tested a possible translational control of *sox21a* and *myc* in ISCs by Aub. Indeed, damage induced Sox21a (**Fig.4D-F**) and Myc (**Fig.4G-I**) expression was significantly impaired upon *aub* knockdown. Unfortunately, the lack of available antibodies precluded us from taking a similar approach for Socs36E. Altogether, these data suggest that Aub drives regenerative ISC proliferation, at least in part

through cell autonomous upregulation of *sox21a* and *myc* translation and in a manner that is independent of its association with piRNAs.

The multiprotein complex eIF3 is involved in the early steps of protein translation where it actively participates in the formation and stabilisation of the pre-initiation complex but also in the recruitment of mRNAs (Asano et al., 2000, Valásek et al., 2003, MajumdarBandyopadhyay and Maitra, 2003, Jivotovskaya et al., 2006). Previously identified roles of Aub in protein translation involves its physical interaction with components of the early translation machinery, including eIF3 and eIF4 (Ma et al., 2017, Ramat et al., 2020). Consistently, wild type midguts showed significant upregulation of a subunit of the eIF3 complex, eIF3C, in ISCs in response to damage (**Fig.5A, B**). Knocking down different subunits of the eIF3 complex in ISCs mimicked the effect of *aub* downregulation on puromycin incorporation (**Fig.S5D, D'**) and on ISC proliferation during midgut regeneration (**Fig.5C**). Additionally, loss of eIF3C impaired ISC proliferation caused by *aub* overexpression (**Fig.5D**).

We next tested a potential epistatic relationship between eIF3C and the expression of Sox21a and Myc in regenerating ISCs. Unexpectedly, *eIF3C* knockdown did not impact the damage-induced upregulation of either Sox21a or Myc expression in ISCs (**Fig.5E-J**). Similarly, the loss of Sox21a or Myc did not decrease eIF3C expression (**Fig.5K** and **Fig.S5E-G**), suggesting that the regulation of Sox21a and Myc by Aub in ISCs does not involve the eIF3 complex (**Fig.5L**). Further work will be necessary to fully understand the mechanisms of cell signalling regulation by Aub in ISCs and identify specific targets of eIF3C in the system.

The human homologue of Aub, *PIWIL1,* is upregulated in colorectal cancer.

Aberrant expression of human *PIWIL1* has been reported in colorectal (Sellitto et al., 2019, Wang et al., 2015a, Sun et al., 2017) and gastric cancers (Araújo et al., 2018, Shi et al., 2020) where *in vitro* studies in 2D cell cultures suggest its role in cell proliferation, cell migration, invasiveness and tumourigenesis. Consistently, our analysis of *PIWIL1* gene expression in colon tissue samples using the TNMplot tool (Bartha and Győrffy, 2021) (**Fig.6A-C**) revealed a significantly higher *PIWIL1* gene expression in colon adenocarcinoma versus normal non-paired tissues (**Fig.6A**) as well as versus adjacent normal tissues (**Fig.6B**). Chip-seq data analysis with the TNMplot tool also revealed strong overexpression of *PIWIL1* in metastatic tissues

(**Fig.6C**). We next took advantage of the publicly available transcriptomic data from the Cancer Genome Atlas Program (TCGA, PanCancer Atlas) and analysed *PIWIL1* expression across different CRC subtypes (CMS1-4) as classified by (Guinney et al., 2015) (**Fig.6D**). Interestingly, *PIWIL1 gene* expression was significantly upregulated in the CMS1 human CRC subtype (**Fig.6D**), which presents high microsatellite instability correlated with hypermethylated profiles and a strong immune activation (Guinney et al., 2015). Consistently, we observed significant *PIWIL1* upregulation in patients with tumours characterised by high microsatellite instability (**Fig.6E**). Next, we assessed levels of PIWIL1 in tissue microarrays from a local cohort of CRC patients who had undergone elective and potentially curative resection of stage I-III colorectal adenocarcinoma in a single surgical unit at the Glasgow Royal Infirmary, Western Infirmary or Stobhill Hospitals (Glasgow, UK) between 1997 and 2007. First, we confirmed PIWIL1 antibody specificity in testis from wild type and *Piwil1* mutant mice (**Fig.S6A**). In line with previous reports, we observed strong expression of PIWIL1 in multiple CRC patient samples (**Fig.6F**) and a significant correlation between PIWIL1 levels and poor patient survival (**Fig.6G**). Combined, these results show a strong correlation between high PIWIL expression levels and CRC with potential selectivity towards tumour subtypes.

Aub regulates Wnt and MAPK signalling driven intestinal hyperplasia *in vivo*.

Current knowledge on the role of PIWI in intestinal cancer is largely based on tissue culture work. Oncogenic intestinal hyperplasia can be recapitulated in the adult *Drosophila* intestine *in vivo* through stem cell specific oncogene activation or tumour suppressor knockdown (Lee et al., 2009, Bangi et al., 2016, Jiang et al., 2011, Cordero et al., 2012a). Our previous results in the regenerating midgut suggest that Aub is functionally linked to the Wnt pathway through Myc (**Fig.4G-I**). We therefore used genetically defined fly models to address the *in vivo* role of PIWI proteins in CRC, with a focus on Aub. We first looked at Aub expression in intestinal hyperplasia driven by hyperactivation of Wnt signalling activity, a major driver of early intestinal tumourigenesis, including hereditary familial adenomatous polyposis (FAP) (Segditsas and Tomlinson, 2006). Immunofluorescence staining for Aub showed a significant increase of protein expression in ISCs/EBs from adult midguts where Wnt signalling is hyperactivated upon loss of *Adenomatous polyposis Coli* (*Apc1)* (Lee et al., 2009, Cordero et al., 2012a) (**Fig.7A-C**). We next used the

MARCM system (Lee and Luo, 1999) to induce 10 day-old control (*LacZ*) or *Apc1* mutant clones in the presence or absence of *aub* knockdown (*aub*^{RNAi}) and quantified tumourigenic ISC proliferation by measuring the size of the clones (**Fig.7D-E**). As shown before (**Fig.S1B-C**), knocking down *aub* was not sufficient to impact homeostatic clonal growth (**Fig.7D-E**). In line with our previous report (Cordero et al., 2012a), loss of functional *Apc1* induced a significant increase of clonal size (**Fig.7D-E**). Combined loss of functional *Apc1* and *aub* knockdown led to a complete suppression of *Apc1* clonal growth (**Fig.7D-E**) suggesting that Aub mediates intestinal tumourigenesis by *Apc1*. Activation of Wnt signalling through the upregulation of the Wnt ligand Wingless (Wg) is necessary and sufficient to drive ISC proliferation in adult midguts (Cordero et al., 2012b, Cordero et al., 2012a, LinXu and Xi, 2008). Consistently, knocking down *aub* suppressed ISC proliferation induced by the overexpression of Wg in adult midgut ISCs/EBS (**Fig.7F**).

Our previous analysis pointed to a selective upregulation of *PIWIL1* in CMS1 CRC tumour subtypes (**Fig.6D**). In addition to high microsatellite instability and strong immune activation, CMS1 tumours are characterized by the presence of activating mutations in the EGFR/MAPK signalling component BRAF (Guinney et al., 2015). The functional association between Aub and Sox21a is consistent with a link between Aub and MAPK signalling in intestinal regeneration (Meng and Biteau, 2015)(**Fig.4D-F**). We therefore used MAPK signalling driven fly models of intestinal hyperplasia to address the functional role of Aub in such genetic tumour settings. Overexpression of a constitutively active form of human BRAF (*Raf*^{GOF}) in ISCs/EBs drives robust ISC hyperproliferation in the adult *Drosophila* midgut (**Fig.7G, H, J**) (Brand and Perrimon, 1994, Markstein et al., 2014) and high levels of Aub (**Fig.7H, I**). However, concomitant short-term (2 days) knockdown of *aub* by RNAi in these midguts was insufficient to affect hyperplasia caused by *Raf*^{GOF} (**Fig.7J**). This is likely due to the rapid and very high ISC hyperproliferation induced by *Raf*^{GOF}*,* and the diminished RNAi efficiency to knock down *aub,* as evidenced by the only partial impact of similar gene knockdown timelines on regenerative ISC proliferation (**Fig.S6B)**. We then tried longer periods of transgene co-expression, which allowed for more effective *aub-RNAi* function (**Fig.S6C**). Longer periods (3 days) of *Raf*^{GOF} overexpression had detrimental effects on gut integrity, including decreased ISC proliferation, likely due to high apoptosis (**Fig.7K, L and Fig.S6D**). Unexpectedly, co-expression of *aub RNAi* in such context maintained high levels of ISC proliferation

and impaired apoptosis in *Raf*^{GOF} overexpressing midguts (**Fig.7K, L and Fig.S6D**). We observed a similar phenomenon when knocking down *aub* in midguts with sustained *Ras* hyperactivation (**Fig.S6E-G**). Of note, while we could induce *Ras* hyperactivation in midgut ISCs/EBs for longer periods of time (7 days), this was not possible in the case of *Raf*^{GOF} due to catastrophic tissue disruption.

Altogether, our data suggest a context-dependent role of Aub in tumourigenesis, which may be dictated by the genetic characteristics of the tumour. Importantly, we provide valuable paradigms for broader studies on the role of PIWI proteins and piRNAs in intestinal physiology and tumourigenesis.

Discussion

Multiple lines of evidence have demonstrated roles of PIWI proteins beyond their well-defined function as repressors of TEs expression, including post-transcriptional control of gene expression in the germline and embryo (Barckmann et al., 2015, Dufourt et al., 2017, Ramat et al., 2020, Becalska et al., 2011, WilsonConnell and Macdonald, 1996, Cook et al., 2004, Ma et al., 2017, Rojas-Ríos et al., 2017, Harris and Macdonald, 2001). Here, we discover a new role of Aub in the adult midgut, which is uncoupled of its piRNA regulatory function and involves translational regulation of conserved pro-regenerative transcription factors within intestinal stem cells.

Aub acts as a regulator of protein translation in ISCs.

Our work underscores a central role of inducible protein synthesis in the capacity of stem cells to trigger the regenerative response of the intestine following damage **(Figs.4 and Fig.5)**. This includes increased Aub production itself **(Fig.1)** and the upregulation of a core component of the translation initiation machinery eIF3 **(Fig.5).** Physical interaction with translation initiation factors mediates the role of Aub in post-transcriptional gene regulation through binding to specific mRNAs in the germline and ovaries (Ma et al., 2017, Ramat et al., 2020). Unexpectedly, direct interaction between Aub and eIF3 seems unlikely in midgut ISCs, as suggested by the distinct regulation of Sox21a and Myc in ISCs by Aub but not eIF3c (**Figs.4** and **5**). Our results therefore reveal not only a role Aub in protein translation beyond the mainstream pathway involving eIF3, but also the existence of, yet to be identified, eIF3 target mRNAs within ISCs, which are essential for intestinal regeneration. Differential requirement of translation initiation factors and target specific mRNA translation by the eIF3 complex regulate developmental processes in *Drosophila* and mice (Fujii et al., 2021, Rode et al., 2018). Further studies will be needed to determine by which mechanisms Aub regulates Sox21 and Myc in ISCs. Regulation of germline stem cell self-renewal and differentiation by Aub has also been linked to physical interaction with subunits of the eIF4 translation initiation complex (Ma et al., 2017). It is therefore possible that a similar functional relationship exists between Aub and eIF4 in ISCs. However, the reduced abundance of midgut piRNAs relative

to the germline, and current lack of *in vitro* cultured systems to increase tissue mass, complicates the implementation of classical molecular and biochemical approaches used in the PIWI/piRNA field for characterization of protein/protein and protein/RNA interactions in ISCs.

What drives the observed upregulation of Aub in ISCs **(Fig.1)** is unknown. Intriguingly, analysis of protein/mRNA complexes in the germline revealed Aub binding to its own mRNA (Ma et al., 2017). While we don't find significant global changes in *aub* mRNA in the midgut **(Fig.1)**, it is worth considering the possible existence of an auto-regulatory mechanism of Aub regulating its own production in ISCs. Additionally, stress signals commonly involved in driving regenerative and tumourigenic ISC proliferation could be playing a role in Aub induction.

Aubergine functions independently of piRNAs in ISCs of the adult *Drosophila* midgut.

While multiple studies have demonstrated dependency on piRNA binding for broad functions of Aub, including regulation of mRNA localisation, stability and translation (Barckmann et al., 2015, Dufourt et al., 2017, Rojas-Ríos et al., 2017, Rouget et al., 2010, Ramat et al., 2020, Vourekas et al., 2016, Rojas-Ríos et al., 2023), piRNA-independent roles of PIWI proteins are only recently emerging (Ma et al., 2017, Shi et al., 2020, Li et al., 2020, Tang et al., 2023). Our experiments suggest that the role of Aub in adult *Drosophila* ISC proliferation does not involve its piRNA regulatory function (**Fig.3**). Additionally, loss of function of *ago3*, an essential ping-pong partner of Aub in germline piRNAs biogenesis, did not impact ISC proliferation (**Figs.1** and **Fig.S1**). On the other hand, we showed that the ping-pong pathway component Vasa is required to drive ISC proliferation during midgut regeneration (**Fig.S1**). However, biological functions of Vasa extend beyond its role in the piRNA pathway, including the regulation of cell cycle genes (Yajima and Wessel, 2011), which could potentially explain its role in *Drosophila* ISC proliferation. Alternatively, but less likely, Vasa may physically interact with Aub to regulate ISC proliferation without the need of piRNA binding. Nonetheless, given that Aub is considered essential for ping-pong piRNAs biogenesis in the germline, our results suggesting its dispensability for the ping-pong piRNAs observed in ISCs was unexpected **(Fig.2)**. This could be explained by either a sufficiency to fulfil this role with residual levels of Aub expected from RNAi partial knockdown, or by a non-

canonical Piwi and Ago3 dependent regulation of ISC ping-pong piRNAs in the absence of Aub.

Our results do not exclude a general role of piRNAs in ISCs. Previous reports highlighted the functional role of Piwi in ISC maintenance and TE regulation in ageing intestines (Sousa-Victor et al., 2017). Here, we report the presence of piRNAs in ISCs/EBs and a decrease of regenerative ISC proliferation upon the knockdown of Piwi and other components of the primary piRNA pathway (**Figs.1 and Fig.S1**). Further studies will be needed to directly address the role of PIWI proteins and piRNA biogenesis within ISCs.

Unlike in sorted ISCs/EBs (**Fig.2**), small RNA sequencing of whole midguts shows an overall decrease in the global piRNA signature of the midgut from *aub* mutant animals (**Fig.S2**). Independent reports of *aub* expression in the midgut include enteroendocrine cell progenitors (Korzelius et al., 2019). These results suggest the interesting prospect of a piRNA-dependent regulatory role of Aub in the midgut epithelium or associated tissues.

Aubergine and PIWI proteins in colorectal cancer.

Our initial observations suggest that, while the upregulation of Aub is a common feature of regenerative and oncogenic ISC hyperproliferation, the functional role of PIWI proteins in tumourigenesis is complex and likely context dependent **(Fig.7)**.

Alterations of the protein translation machinery is a cancer hallmark (Song et al., 2021). Over 95% of human CRC cases bear loss of function mutations in the tumour suppressor *APC,* leading to Wnt pathway hyperactivation and the subsequent upregulation of its target gene *myc* (SchatoffLeach and Dow, 2017). Myc expression in CRC relies on the activity of the eukaryotic initiation factor eIF4E (Wiegering et al., 2015, Knight et al., 2021) and eIF4A1 (Waldron et al., 2023). It is therefore possible that the mechanisms mediating the pro-proliferative function of Aub in intestinal regeneration **(Figs.4 and 5)** may extrapolate to pro-oncogenic roles of PIWI proteins in tumours with hyperactivating mutations in Wnt signalling components **(Fig.7)**.

On the other hand, upregulation of Aub upon MAPK signalling hyperactivation revealed a pro-apoptotic/tumour suppressive role of Aub in such context **(Fig.7),** which may predict a similar functional outcome for upregulated *PIWIL1* in CMS1

tumour subtypes containing BRAF hyperactivation **(Fig.6)** (Guinney et al., 2015)**.** Anti- and pro-apoptotic roles have been described for PIWIL1 in tumour stem cells, including glioma and leukaemia (Wang et al., 2015d, Huang et al., 2021). Our results may therefore reveal general mechanisms mediating dual and antagonistic functions of PIWI proteins in cancer.

Additional features of CMS1 tumours include epigenetic modifications, such as genome hypermethylation (Guinney et al., 2015). PIWI proteins induce transposon silencing partly through DNA hypermethylation, a function that might be repurposed in oncogenic settings through the hypermethylation of tumour gene promoters (WajedLaird and DeMeester, 2001). Previous studies have linked PIWI proteins to DNA hypermethylation in tumourigenesis and cell invasion in sarcoma and melanoma, respectively (SiddiqiTerry and Matushansky, 2012, Wang et al., 2015c). PIWIL1 expression also correlates with promoter methylation of the tumour suppressor gene PTEN in endometrial cancer (Chen et al., 2015). Further *in vivo* studies in genetically defined tumour models would provide invaluable insights into the role of PIWI proteins and piRNAs in colorectal cancer and our work presents excellent paradigms to achieve this.

Material and Methods

A complete list of fly stocks, full genotypes, and reagents used in this study can be found in Supplementary Table #1.

Drosophila melanogaster stock rearing and maintenance.

Fly stocks were kept in temperature and humidity-controlled incubators set up with a 12h-12h light/dark cycle. For experiments with *aub* mutant lines, crosses were performed at 25°C and the desired F1 progeny was sorted 2/3 days after adult eclosion and kept at 25°C for 5-7 days before dissection. For experiments using the *GAL4*/*GAL80*^{ts} system, flies were crossed at 18°C. The desired F1 progeny was sorted 2/3 days after adult eclosion and was kept at 18°C for 5 days before being transferred to 29°C to allow transgene activation. The incubation time at 29°C varied from 2 days to 10 days depending on the transgene. In all cases, experimental flies were flipped every two days on fresh food. Only mated females were used for experiments.

Human patient information and ethics statement.

The human cohort analysed contains 1030 colorectal cancer (CRC) patients who had undergone elective and potentially curative resection of stage I-III colorectal adenocarcinoma in a single surgical unit at the Glasgow Royal Infirmary, Western Infirmary or Stobhill Hospitals (Glasgow, UK) between 1997 and 2007. Resection was considered curative based on pre-operative computed tomography and intra-operative findings. The data are stored within the Glasgow Safehaven (GSH21ON009) and ethical approval was in place for the study (MREC/01/0/36).

Damage-induced intestinal regeneration.

To induce intestinal regeneration, mated female flies were fed on filters (Whatman) soaked in 5% sucrose only (control condition) or with the pathogenic bacteria *Pseudomonas entomophila* (*Pe*) at OD_{600}=25 (damage condition) for 16 hours prior to dissection. The bacterial solution was obtained after overnight culture in LB medium at 29°C under 220 rpm shaking overnight, after which bacteria were pelleted

(Beckman Coulter JS-4.2 rotor, 10 min, 4000 rpm) and diluted in a solution of 5% sucrose to reach OD_{600}=25.

Immunohistochemistry.

Drosophila tissue: The dissection of guts was performed in PBS at room temperature and 16 hours after feeding the mated female flies with sucrose or *Pe*. After dissection, guts were immediately fixed in a solution of 4% paraformaldehyde (Polysciences Inc) for 1 hour. Guts were then washed in PBST (PBS with Triton 0.2%) before incubation overnight at 4°C with the primary antibodies diluted in blocking solution PBT (with 0.5% BSA). The day after, guts were washed 3x15 minutes with PBST at room temperature before incubation with the secondary antibodies for 2 hours at room temperature. Guts were then washed 3x15 minutes with PBST at room temperature before mounting in DAPI containing mounting medium. Slides were kept at 4°C before imaging. To improve Aub, Dcp-1, eIF3C and Myc staining, guts were placed in methanol for 10 minutes at room temperature after the fixation step with 4% paraformaldehyde.

Human and mouse tissue: Immunohistochemistry (IHC) staining was performed on a previously constructed human tissue microarray or on 4µm formalin fixed paraffin embedded sections, which had previously been incubated in a 60□C oven for 2 hours. Tissue slides for PIWIL1 detection were stained on a Leica Bond Rx Automated Stainer. Samples underwent on-board dewaxing and epitope retrieval using ER2 solution (Leica) for 20 minutes at 95°C. Sections were rinsed with Leica wash buffer before peroxidase blocking was performed using an Intense R kit (Leica) for 5 minutes. Sections were rinsed with wash buffer (Leica) before anti-PIWIL1 application at an optimal dilution (1/200). The sections were then rinsed with wash buffer (Agilent) for 30 minutes, before secondary antibody application. The sections were rinsed with wash buffer, visualized using DAB and counterstained with Haematoxylin in the Intense R kit. To complete the IHC staining sections were rinsed in tap water, dehydrated through a series of graded alcohols, and placed in xylene. The stained sections were cover slipped in xylene using DPX mounting medium.

Details of antibodies sources and concentrations used as well as reagent' information can be found in Supplementary Table #1.

Generation of *aub* transgenes.

The three pUASt-attB-GFP constructs of *aub* were generated for this study. A complementary DNA (cDNA) of *aub* was amplified from w^{1118} flies and cloned into the pUASt-attB plasmid, that was originally made by the Basler group (GenBank accession EF362409, PUBMED: 17360644) and received as a gift from Julius Brennecke. A GFP cDNA was inserted N-terminally to *aub* cDNA. Standard site-directed mutagenesis by Phusion DNA Polymerase (Thermo Fisher) was used to introduce amino acid substitutions to generate aub^{AA} (Y345A/Y346A, (Barckmann et al., 2015)) and aub^{ADH} (D636A, (Wang et al., 2015b)). Plasmid construction and sequences are available at https://github.com/RippeiHayashi/gut_aubergine.

Egg laying/eclosion assay.

Crosses to obtain experimental animals were kept at 18□C. Virgin females of the desired genotype were selected and placed into fresh vials and allowed to mate with w^{1118} males. A maximum of 5 females and 5 males were housed in each vial and allowed to mate over a period of 24 hours at 18□C. The following day, males were removed, and females were moved onto fresh food and incubated at 25□C. Females were flipped into new vials every 24 hours. The number of eggs in each vial was counted and recorded at the same time. This process was repeated 3 more times. Importantly, the number of live females was recorded each time, at the time of flipping. Any females that died during the night were included in the eggs/adult ratio but were excluded from the subsequent recordings. This experiment was repeated three times.

Protein translation assay.

For general protein translation assessment, flies were fed on filters (Whatman) soaked in 5% sucrose only or with *Pe* OD_{600}=25 16 hours prior to gut dissection in Schneider's insect medium (Sigma-Aldrich) containing puromycin (stock solution 25 mg/mL, Sigma-Aldrich) with a final concentration of 25µg (1µL of stock solution) of puromycin in 5mL of Schneider's insect medium. During dissection, Malpighian tubules and crop were kept attached to the gut and precaution was taken to keep the intestines intact. Guts were then incubated at room temperature in puromycin containing medium for 45 minutes. After incubation, we applied the immunochemistry protocols we described in this manuscript.

Clonal analysis.

Crosses were performed at 25°C and parental lines were flipped twice a week. Clones were induced using the MARCM technique (Lee and Luo, 1999). The desired progeny was collected and aged for 3 to 5 days at 25°C before undergoing three 30 minutes heat shocks in one day, in a 37°C water bath. Heat shocked adults were then aged for 10 days at 25°C before dissection.

Fluorescence-activated single cell sorting (FACS).

Control flies and flies expressing RNAi against *aub* were collected between 2 to 3 days after hatching and kept at 18°C for 5 days before being transferred to 29°C. Flies were kept at 29°C for 7 days and were flipped into fresh food vials every two days. Fly guts were dissected in cold PBS 16 hours after animals were fed with 5% sucrose only or 5% sucrose containing *Pe*. The crop, the Malpighian tubules and the hindgut were carefully removed. Midguts were then collected and transferred to an Eppendorf containing 400 µL of PBS and kept on ice. Each Eppendorf contained roughly 100 midguts. Once all the tissue was dissected, 10 µL of elastase (Sigma-Aldrich, 10 µg/ µL) was added to each Eppendorf. Samples were kept at 27°C in a heat block for at least 1 hour until midguts were fully dissociated. Tissues were further disrupted by pipetting up and down every 5 minutes. Samples were then centrifuged at 300 rcf for 20 minutes at 4°C. After removing the supernatant, the pellet was resuspended in cold PBS. To eliminate enterocytes as much as possible, the cell suspension was filtered with a 30 µm filter (Sysmex). 500 µL of cold PBS were added to wash the filter. After filtration, samples were ready for sorting. Sorting was performed by the CRUK Scotland Institute flow cytometry facility on a FACSAria Fusion Flow Cytometer (BD Biosciences). GFP or Red stinger positive controls were used to set up the flow cytometer parameters that were used for all the conditions. In parallel to the sorting, a few microliters of samples were taken and stained with 20 µL of DAPI to visualize cell death. Between 250 and 500 flies were dissected per condition, resulting in 250,000 to 750,000 sorted cells. Three biological replicates were dissected for each condition. Sorted cells were pelleted by centrifugation at 300 rcf for 20 minutes at 4°C. After carefully removing the supernatant, 800 µL of TRIzol (Invitrogen) was added to the samples, followed by RNA extraction and sequencing.

Small RNA sequencing.

Small RNA sequencing was performed on either whole midguts, ovaries or sorted ISCs/EBs. For small RNA preparation from whole midguts, flies were dissected in cold PBS 16 hours after being fed with 5% sucrose only or 5% sucrose containing *Pe*. The crop, the Malpighian tubules and the hindgut were carefully removed. Three replicates of 40 midguts each were dissected for each condition. Guts were then collected and transferred to an Eppendorf containing 400 µL of PBS and kept on ice. Once all the tissue was dissected, 10 µL of elastase (Sigma-Aldrich, 10 µg/µL) was added to each Eppendorf. Samples were kept at 27°C in a heat block for at least 1 hour until the guts were totally degraded. Tissues were disrupted by pipetting up and down every 5 minutes. Samples were then centrifuged at 300 rcf for 20 minutes at 4°C. After removing the supernatant, the pellet was resuspended in 800 µL of TRIzol (Invitrogen). The same protocol was applied for the ovaries. Approximately 10 pairs of ovaries were dissected. We generated small RNA libraries from 1 ~ 5 µg of total RNA using a modified protocol from the original method (Hafner et al., 2008). 19 to 35 nucleotides-long RNA was first selected by polyacrylamide gel electrophoresis (PAGE) with 7M Ureal using radio-labelled 19mer (5′′-CGUACGCGGGUUUAAACGA) and 35mer spikes (5′′-CUCAUCUUGGUCGUACGCGGAAUAGUUUAAACUGU). The size-selected RNA was precipitated, oxidised by sodium periodate (Sigma)(Akbergenov et al., 2006), and size-selected for the second time by PAGE. The size-selected oxidised small RNAs were then ligated to the 3' adapter from IDT (5rApp/NNNNAGATCGGAAGAGCACACGTCT/3ddC where Ns are randomised) using the truncated T4 RNA Ligase 2, truncated KQ (NEB), followed by a third PAGE to remove non-ligated adapters. Subsequently, the RNA was ligated to the 5' adapter from IDT (ACACUCUUUCCCUACACGACGCUCUUCCGAUCUNNNN where Ns are randomised) using the T4 RNA Ligase 1 (NEB). Adapter-ligated RNA was reverse-transcribed using SuperScript II (Thermo Fisher) and amplified by KAPA LongRange DNA polymerase (Sigma, KK3502) using the universal forward primer, Solexa_PCR-fw: (5′-AATGATACGGCGACCACCGAGATCTACACTCTTTCCCTACACGACGCTCTTCCGATCT) and the barcode-containing reverse primer TruSeq_IDX: (5′-CAAGCAGAAGACGGCATACGAGATyyyyyyGTGACTGGAGTTCAGACGTGTGCTCTTCCGATCT where yyyyyy is the reverse-complemented barcode sequence).

Amplified libraries were multiplexed and sequenced on a HiSeq platform in the paired-end 150 bp mode by GENEWIZ/Azenta.

Small RNA sequencing analysis.

The R1 sequencing reads were trimmed of the Illumina-adapter sequence using the FASTX-Toolkit from the Hannon Laboratory (CRUK Cambridge Institute). The 4 random nucleotides at either ends of the read were further removed. The trimmed reads of 18 to 40 nt in size were first mapped to the infrastructural RNAs, including ribosomal RNAs, small nucleolar RNAs (snRNAs), small nuclear RNAs (snoRNAs), microRNAs, and transfer RNAs (tRNAs) using Bowtie 1.2.3 allowing up to one mismatch. Sequences annotated in the dm6 r6.31 assembly of the *Drosophila melanogaster* genome were used. The trimmed and unfiltered reads were then mapped to the dm6 genome using Bowtie allowing up to one mismatch. Reads that uniquely mapped to the genome were analysed for the tile analysis. Reads that mapped to the 100 nt upstream and downstream genomic regions of tRNA, snRNA and snoRNA insertions as well as those that mapped to the *aubergine* gene locus were removed from the tile analysis. Bedtools 2.28.0 was used to count the coverage of the mapped reads. Endogenous siRNA reads (annotated as hpRNA) were used for normalisation. The trimmed and unfiltered reads were separately mapped to the curated sequences of *Drosophila melanogaster* transposons (Senti et al., 2015) using Bowtie allowing up to three mismatches with the option of --all --best --strata. The size distribution of the transposon-mapping reads was made using ggplot2 3.4.4 in R 4.0.0. Nucleotide frequencies around the first nucleotide position of antisense and the tenth nucleotide position of the sense transposon-mapping piRNA reads (longer than 22 nucleotides) were counted and visualised using weblogo 3.7.8. Frequencies were measured in the window of 11 nucleotides and the z scores were calculated as the deviation of the frequency value at the first (antisense reads) and tenth (sense reads) positions from the mean frequency divided by the standard deviation of the frequencies. Small RNA sequencing libraries from Siudeja et al. (Siudeja et al., 2021) were analysed in the same way except for using the adapter sequence TGGAATTCTCGGGTGCCAAG, and not trimming the 4 nucleotides at either end.

PolyA-selected RNA sequencing.

Polyadenylated RNA was purified from the DNase-treated total RNA using oligo d(T)25 magnetic beads (NEB, S1419), and then used for the library preparation. Libraries were cloned using the NEBNext Ultra Directional II RNA Library Prep Kit for Illumina (NEB, E7760), following the manufacturer's instruction, and amplified by KAPA polymerase using the same primers as for the small RNA sequencing.

PolyA-selected RNA analysis.

Both R1 and R2 reads from the polyA-selected RNA sequencing reads were trimmed of the Illumina-adapter sequences using the FASTX-Toolkit. The trimmed reads were subsequently filtered by the sequencing quality. Only the paired and unfiltered reads were then mapped to the dm6 r6.31 transcriptome combined with curated sequences of *Drosophila melanogaster* transposons using salmon/1.1.0 with the options of --validateMappings --incompatPrior 0.0 --seqBias --gcBias. Length-normalised transposon mRNA reads per one million transcripts including host mRNAs were compared between different libraries. polyA-selected RNA sequencing libraries from ovarian samples from Senti et al. (Senti et al., 2015) were also analysed in the same way.

***Drosophila* RNA extraction and RT-qPCR.**

Total RNA was extracted from tissues dissected in cold PBS. Three or four replicates of 20 to 40 guts were dissected for each condition. Depending on the experiments, whole guts or only R4-R5 regions were dissected. Ovaries were also dissected in parallel as a positive control. Tissues were homogenised in 100 µl of Trizol (Thermo Fischer Scientific) using a mortar and a pestle first, followed by adding further 700 µl of Trizol. 200 µl of Chloroform was added and mixed well with Trizol by vortexing before centrifugation on a bench top centrifuge. The aqueous phase was saved, and RNA was precipitated with iso-propanol. RNA was treated with DNase (Thermo Fischer Scientific) and quantified using a NanoDrop Spectrophotometer. About 1 µg of RNA was converted to cDNA using a high-capacity cDNA reverse transcription kit (Thermo Fisher Scientific). RT-qPCR was performed using Perfecta SYBR green fast mix (Quantabio) as per the manufacturer's instructions on an Applied Biosystems QuantStudio 3 fast real-time PCR system and each reaction was carried out in triplicate. A standard curve was created using 1:10 dilutions from pooled cDNA samples. The amount of sample was extrapolated from this standard curve and

normalised using data from the housekeeping gene *rpl32*. Melting curves were generated previously to ensure only one product was formed from each pair of primers. Data were exported and analysed in Excel. The results are shown as the ratio of average of mRNA levels of the candidate gene/*rpl32*.

TCGA analysis.

To study *PIWIL1* RNA expression across the different CMS of CRC or according to the microsatellite status of the patients, we took advantage of the TCGA datasets from the PanCancer Atlas. Analysis has been performed on open access data from colonic adenocarcinoma patients only. Differential gene expression was then assessed, and statistics have been performed using Graphpad.

Sample visualization and image acquisition.

PH3-positive cells counting was performed using a BX51 Olympus. Fluorescence images of *Drosophila* intestines were acquired using a confocal Zeiss 710 or a Zeiss LSM 780. Stained TMAs slides were scanned and analysed using the HALO system (indica labs).

TMA Scoring.

Scoring of PIWIL1 expression in the cytoplasm was independently performed by two examiners (K.B and L.R.C) blinded to clinical data. PIWIL1 score was individually determined in the cytoplasm using the equation: 0 × (% cells not stained)□+□1 × (% cells weakly stained)□+□2 × (% cells moderately stained)□+□3 × (% cells strongly stained). This method gave a range of scores from 0 to 300. Damaged samples and samples with tumour tissue representing less than 10% of the total tissue were excluded.

Quantification and statistics.

Quantification of ISC proliferation and apoptosis was done by manually counting the number of PH3-positive cells per posterior midguts and by manually counting the number of Dcp-1-positive cells in the lumen per image, respectively. Quantification of eIF3C, Myc, puromycin and Sox21a staining was performed by measuring the mean fluorescence intensity of the protein in all GFP positive cells on a SUM projection realised via Fiji (ImageJ 2.14.0/1.54f). Prior to the measurement, a mask was

created via Fiji to delineate the GFP positive cells only, using the tool “Create a selection”. In parallel, mean fluorescence intensity of the background was measured on a specific region of interest on each SUM projection and subtracted from the signal measured in the cells.

Quantification of Aub staining was performed by measuring the mean fluorescence intensity per cell on a SUM projection done by Fiji. This measure was blindly performed in three different GFP positive cells per gut for Aub. In parallel, mean fluorescence intensity of the background was measured on a specific region of interest on each SUM projection and subtracted from the signal measured in the cell. This quantification was repeated in 5 different guts per biological replicate. A minimum of 3 biological replicates per condition were quantified.

In the rescue experiments (*aub*^{WT}, *aub*^{AA} and *aub*^{ADH}), GFP and Aub stainings were quantified by measuring the mean fluorescence intensity of the protein in all GFP positive cells on a MAX projection realised via Fiji. Prior to the measurement, a mask was created on Fiji to delineate the GFP positive cells only via using the tool “Create a selection”. In parallel, mean fluorescence intensity of the background was measured on a specific region of interest on each SUM projection and subtracted from the signal measured in the cells.

Quantification of ISC proliferation in MARCM clones was performed by manually counting the number of DAPI positive cells in each GFP-positive clone. The statistics were done with GraphPad Prism 6. The tests used for each experiment are described in the figure legends.

For TMAs analysis, the cut off value for high and low expression of PIWIL1 was determined using the Survminer package in RStudio software version 1.4. Patients were excluded from analysis if mortality occurred within 30 days post-surgery, upon presence of metastatic stage disease, and/or if subject to administration of neoadjuvant therapy. Kaplan Meier survival analysis and univariate cox regression analysis were performed using SPSS version 8 (IBM) to determine the association between expression of PIWIL1 and cancer-specific survival.

Acknowledgements

We would like to thank Allison Bardin; Benoit Bîteau; Julius Brennecke; Angela Giangrande; Ginés Morata; Yulii Shidlovskii and Phillip Zamore for generously sharing flies and reagents. We thank the Bloomington Drosophila Stock Center; the Vienna Drosophila Resource Center and the *Drosophila* Studies Hybridoma Bank for fly stocks and antibodies. We would like to thank the Core Services and Advanced Technologies at the CRUK Scotland Institute, which is core funded by Cancer Research UK (A31287). With particular thanks to Leo Carlin, Claire Mitchell and Peter Thomason from the Beatson Advanced Imaging Resource; Yi-Hsia Liu and Thomas Gilbey from the FACS facility and Colin Nixon and the Histology Laboratory for assistance with mouse and human tissue sample preparation and staining. We are grateful to Henri Jasper and Pedro Souza-Victor for their advice and help with cell sorting and mRNA sequencing of midgut ISCs/EBs. We thank all members of the Cordero laboratory for general advice on the project.

Human tumour sample analysis was performed on data generated by the TCGA Research Network: https://www.cancer.gov/tcga.

The manuscript was critically reviewed by Catherine Winchester (CRUK Scotland Institute).

Funding

Work in the Cordero laboratory is funded through a Wellcome Trust and Royal Society Sir Henry Dale Fellowship (104103/Z/14/Z), and Wellcome Trust Senior Research Fellowship (223091/Z/21/Z) to J.B.C., core Institutional funds from CRUK to the CRUK Scotland Institute (A31287) and a China Scholarship Council studentship to Y.T. (202006910022). Research in the Hayashi laboratory is supported by the Australian Research Council (DP210102385). The Edwards laboratory is funded by Chief Scientific Office grants (CSO EPD/22/13; K.P. and J.E.) (CSO TCS/22/02; J.E.) and CRUK funding to the CRUK Scotland Centre (CTRQQR-2021\100006). The Gontijo and Heredia laboratory was supported by the FCT (LISBOA-01-0145-FEDER-030753; 10.54499/CEECINST/00102/2018/CP1567/CT0031; 10.54499/DL57/2016/CP1457/CT0016); EXPL/BIA-BID/1524/2021; EXPL/BIA-

COM/1296/2021; 10.54499/2022.03859.PTDC, 10.54499/UIDB/04462/2020; 10.54499/UIDB/00329/2020, 10.54499/LA/P/0087/2020; 10.54499/LA/P/0121/2020; LISBOA-01-0145-FEDER-022170; UID/Multi/04462/2019.

Conflict of interest

None declared.

Data availability

Sequencing data and processed files have been deposited to Gene Expression Omnibus: GSE253621 (small RNA sequencing); GSE253624 (mRNA sequencing). Codes for the computational analyses are available at https://github.com/RippeiHayashi/gut_aubergine.

Author contributions

K.B., L.R.C., R.H and J.B.C design the experiments. K.B., L.R.C., Y.T., Y.Y., A.R.C. and R.H. performed the experiments. K.B., L.R.C., R.H. and J.B.C. analysed the data. K.A.P. and J.E. provided methodology for TMA analysis. F.H. and A.M.G. generated, *aub*^{NH2} recombinant fly line. K.B. wrote the original manuscript draft. K.B., R.H. and J.B.C. wrote, reviewed, and edited the manuscript.

Figure legends

Figure 1: Aub is required for the proliferation of ISCs in response to intestinal damage.

(A) Representative confocal image of a mated female adult *Drosophila*'s gastrointestinal tract. ISCs and EBs are identified with GFP (green). Dashed yellow lines delineate the posterior midgut. Scale bar is 200µm. **(A')** Representative scheme of the *Drosophila* intestinal epithelium and associated tissues. ISCs, intestinal stem cells; EBs, enteroblasts; EEPs, enteroendocrine cell precursors; ECs, enterocytes; EEs, enteroendocrine cells; VM, visceral muscle; EN, enteric neurons; TTC, terminal tracheal cell. **(B)** RT-qPCR for mRNA expression of the PIWI genes *aub*, *piwi* and *ago3* in the R4-R5 midgut region (pink), the whole adult *Drosophila* midgut (red), and adult *Drosophila* ovaries (green) relative to *rpl32* mRNA levels. Number of biological replicates is 3 with each replicate containing 20 to 40 midguts/R4-R5 regions dissected. **(C)** Representative confocal images of PH3 staining (green) in the posterior midguts of w^{1118}, $piwi^{1}/piwi^{2}$, aub^{QC42}/aub^{HN2} and ago^{t2}/ago^{t3} from whole mutant female flies fed with sucrose or *Pe*. Scale bar is 100µm. **(D)** Quantification of PH3-positive cells in posterior midguts as in (C). n = number of midguts/flies quantified. **(E)** Quantification of PH3-positive cells in the posterior midguts of w^{1118}, $aub^{G1/G2}$ and $aub^{clash/clash}$ flies fed with sucrose or *Pe*. n = number of midguts/flies quantified. **(F)** Representative confocal images of PH3 staining (green) in the posterior midguts of flies expressing GFP in ISCs/EBs, aub^{RNAi} alone or overexpressing aub^{RNAi} within ISCs/EBs and fed with sucrose or *Pe*. Scale bar is 100µm. **(G)** Quantification of PH3-positive cells in the posterior midguts as in (F). n = number of midguts/flies quantified. **(H, I)** Representative confocal images of Aub staining (red) in the posterior midguts of flies expressing GFP only **(H)** or with aub^{RNAi} **(I)** within ISCs/EBs (green) and fed with sucrose or *Pe*. Dashed yellow squares delineate the magnified area shown in the right panels. Scale bar is 50µm. **(J)** Quantification of Aub staining within ISCs/EBs in the posterior midguts as in (H, I). n = number of cells quantified. 3 cells per gut/fly have been quantified and 10 flies per condition have been analysed. **(K)** RT-qPCR for mRNA expression of *aub* in whole adult *Drosophila* midguts relative to *rpl32* mRNA levels. Number of biological replicates is 4 with 30 midguts dissected per replicate. A Shapiro-Wilk

normality test followed by a Mann-Whitney t test were used. **(L, M)** Quantification of PH3-positive cells in the posterior midguts of flies fed with sucrose or *Pe* and expressing GFP alone or with *aub*^{RNAi} in either EBs **(L)** or ISCs **(M)**.

Unless otherwise noted, two-way ANOVA followed by a Sidak's multiple comparisons test were used for statistical analysis of all data sets. n are indicated below each graph following the same order of the genotypes and treatments presented in the graph. Data represent the mean±s.d. ns, not significant ($P>0.05$); *$P<0.05$, **$P<0.01$, ***$P<0.001$ and ****$P<0.0001$. a.u., arbitrary units. Nuclei are identified with DAPI.

Figure 2: Aubergine does not impact the presence of piRNAs in *Drosophila* intestinal stem/progenitor cells.

(A) Schematic representation of the *Drosophila* intestine. The green dots represent ISCs/EBs that were sorted *via* FACS for small RNA sequencing. **(B, B', C, C')** Size distribution (top graphs) of all transposon-mapping reads and the Uridine- and Adenine-frequencies of transposon-mapping reads of piRNA size (>22nt) (bottom graphs) in oxidized libraries from sorted ISCs/EBs of control flies fed with sucrose or *Pe* **(B, B')** or in oxidized libraries from sorted ISCs/EBs of flies expressing *aub*^{RNAi} in ISCs/EBs and fed with sucrose or *Pe* **(C, C')**. siRNAs are typically sized at 21 or 22nt while piRNAs are longer than 22nt (see dashed black rectangles for higher magnification). Uridine (red) at the 1st base position of TE antisense piRNA reads (>22nt) is a common signature of all piRNAs while Adenine (green) at the 10th base position of TE sense piRNA reads is a signature of Ping-Pong piRNAs. **(D, E)** Quantification of TE antisense **(D)** and sense **(E)** piRNA abundance as in (B, B', C, C'). Two-way ANOVA followed by a Sidak's multiple comparisons test were applied. n = 3 biological replicates. **(F)** Representation of piRNA cluster expression in sorted ISCs/EBs from control flies or from flies expressing *aub*^{RNAi} in ISCs/EBs and fed with sucrose or *Pe,* compared to ovaries. The results are presented relative to control ovaries. Germline clusters 38C left and 42AB are represented in orange and blue, respectively. The somatic cluster flamenco is represented in green.

Data represent the mean±s.d. ns, not significant ($P>0.05$); *$P<0.05$, **$P<0.01$, ***$P<0.001$ and ****$P<0.0001$. a.u., arbitrary units. TE, transposable elements; AS, antisense; S, sense.

Figure 3: Aub regulates intestinal regeneration independently of its piRNA regulatory function.

(A, B) Abundance of TE mRNAs in sorted ISCs/EBs from control flies **(A)** or in flies expressing *aub*^{RNAi} within ISCs/EBs **(B)** and fed with sucrose or *Pe*. TE mRNA counts were normalised to one million transcript counts including host mRNAs (TPM), and Suc versus *Pe* fed conditions were compared. Red dashed lines indicate 4-fold changes in either direction. TE mRNAs shown in red, blue and green represent TE mRNAs highly expressed in the gut, in the ovaries or in both, respectively. **(C)** Representative confocal images of GFP (green) and Aub staining (red) in posterior midguts from control flies or flies expressing *aub*^{WT}, *aub*^{AA} or *aub*^{ADH} within ISCs/EBs. Dashed white lines delineate the posterior midguts. **(D, E)** Quantification of GFP **(D)** or Aub staining **(E)** within ISCs/EBs in the posterior midguts as in (C). A Shapiro-Wilk normality test followed by a Kruskal-Wallis one-way ANOVA and a Dunn's multiple comparisons tests were applied. n = number of midguts/flies quantified. **(F)** Representative confocal images of Aub staining (red) in the posterior midguts of *aub*^{HN2}/*aub*^{QC42} mutant flies expressing *aub*^{WT}, *aub*^{AA} or *aub*^{ADH} within ISCs/EBs and fed with sucrose or *Pe*. Dashed white lines delineate the posterior midguts. **(G)** Quantification of Aub staining within ISCs/EBs in posterior midguts as in (F). **(H)** Quantification of PH3-positive cells in the posterior midguts of control flies; *aub*^{HN2}/*aub*^{QC42} flies expressing GFP alone or with *aub*^{WT}, *aub*^{AA} or *aub*^{ADH} within ISCs/EBs and fed with sucrose or *Pe*. Two-way ANOVA followed by a Sidak's multiple comparisons test were applied in (G) and (H). In both cases, n = number of midguts/flies quantified, which are indicated below each graph following the same order of the genotypes and treatments presented in the graph.

Data represent the mean ± s.d. ns, not significant ($P > 0.05$); *$P < 0.05$, **$P < 0.01$, ***$P < 0.001$ and ****$P < 0.0001$. a.u., arbitrary units. Nuclei are identified with DAPI. Scale bars are 50µm. TE, transposable elements.

Figure 4: Aub regulates core regenerative stem cell factors in the adult midgut.

(A, B) Representative confocal images of puromycin staining (red) in the posterior midguts of flies expressing GFP alone **(A)** or with *aub*^{RNAi} **(B)** within ISCs (green) and fed with sucrose or *Pe*. **(C)** Quantification of puromycin staining within ISCs in the posterior midguts as in (A and B). **(D, E)** Representative confocal images of Sox21a staining (red) in the posterior midgut of flies expressing GFP alone **(D)** or

with *aub*^{RNAi} **(E)** within ISCs (green) and fed with sucrose or *Pe*. **(F)** Quantification of Sox21a staining within ISCs in the posterior midguts as in (D, E). **(G, H)** Representative confocal images of Myc staining (red) in the posterior midguts of flies expressing GFP alone **(G)** or with *aub*^{RNAi} **(H)** within ISCs (green) and fed with sucrose or *Pe*. **(I)** Quantification of Myc staining within ISCs in the posterior midguts as in (G, H). Two-way ANOVA followed by Sidak's multiple comparisons test were applied in (C, F and I). n = number of midguts/flies quantified and are indicated below each graph in the same order of the genotypes and treatments presented in the graph.

Data represent the mean ± s.d. ns, not significant ($P > 0.05$); *$P < 0.05$, **$P < 0.01$, ***$P < 0.001$ and ****$P < 0.0001$. a.u., arbitrary units. Nuclei are identified with DAPI. Scale bars are 50µm.

Figure 5: Aub regulates the multiprotein complex eIF3.

(A) Representative confocal images of eIF3C staining (red) in the posterior midguts of flies expressing GFP within ISCs (green) and fed with sucrose or *Pe*. Dashed white squares delineate the high magnification shown in the right panels. Yellow arrows highlight ISCs. **(B)** Quantification of eIF3C staining within ISCs in the posterior midguts as in (A). A Shapiro-Wilk normality test followed by an unpaired t test were applied. n = number of midguts/flies quantified. **(C)** Quantification of PH3-positive cells in the posterior midguts of control flies expressing GFP alone or with RNAi against different subunits of the eIF3 complex within ISCs. Flies were fed with sucrose or *Pe*. n = number of midguts/flies quantified and are indicated below each graph in the same order of the genotypes and treatments presented in the graph. **(D)** Quantification of PH3-positive cells in the posterior midguts of control flies expressing GFP only; with *aub::GFP* or with *aub::GFP* and *eIF3C*^{RNAi} within ISCs. A Shapiro-Wilk normality test followed by a Kruskal-Wallis one-way ANOVA and a Dunn's multiple comparisons tests were applied. n = number of midguts/flies quantified and are indicated below each graph in the same order of the genotypes and treatments presented in the graph. **(E, F)** Representative confocal images of Sox21a staining (red) in the posterior midgut of flies expressing GFP alone **(E)** or with *eIF3C*^{RNAi} **(F)** within ISCs (green) and fed with sucrose or *Pe*. **(G)** Quantification of Sox21a staining within ISCs in the posterior midguts as in (E, F). **(H, I)** Representative confocal images of Myc staining (red) in the posterior midguts of flies

expressing GFP alone **(H)** or with *eIF3C*^{RNAi} **(I)** within ISCs (green) and fed with sucrose or *Pe*. **(J)** Quantification of Myc staining within ISCs in the posterior midguts as in (H, I). **(K)** Quantification of eIF3C staining within ISCs in the posterior midguts as in (Fig.S5E-G). Two-way ANOVA followed by Sidak's multiple comparisons test were applied for statistical analysis in (C, G, J and K). n = number of midguts/flies quantified and are indicated below each graph in the same order of the genotypes and treatments presented in the graph. **(L)** Current working model on the regulation of regenerative ISC by Aub. ISCs: intestinal stem cells; EBs: enteroblasts, EC: enterocyte; VM: Visceral Muscle; TC: tracheal cell.

Data represent the mean ± s.d. ns, not significant ($P > 0.05$); *$P < 0.05$, **$P < 0.01$, ***$P < 0.001$ and ****$P < 0.0001$. a.u., arbitrary units. Nuclei are identified with DAPI. Scale bars are 50µm.

Figure 6: The mammalian homolog of Aub, PIWIL1, is upregulated in CRC patients.

(A, B) *PIWIL1* expression obtained from RNA sequencing experiments performed in non-paired normal and tumour tissues (**A**) or in paired adjacent normal and tumour tissues (**B**) from human colon adenocarcinoma. Graphs and statistics were done using the TNMplot tool. Mann-Whitney t test was applied. n = number of patients quantified. **(C)** *PIWIL1* expression from ChIP sequencing experiments performed in non-paired normal, tumour and metastatic tissues from human colon adenocarcinoma. Graph and statistics were done using the TNMplot tool. A Kruskal-Wallis one-way ANOVA test was applied. n = number of patients quantified. **(D)** *PIWIL1* expression obtained across 4 CRC subtypes (Guinney et al., 2015) (TCGA, PanCancer Atlas). Shapiro-Wilk normality test followed by a Kruskal-Wallis one-way ANOVA and Dunn's multiple comparisons tests were applied. n = number of patients quantified. **(E)** *PIWIL1* expression according to the microsatellite status of cancer patients (TCGA, PanCancer Atlas). MSS: microsatellite stability; MSI-L: low microsatellite instability; MSI-H: high microsatellite instability. Shapiro-Wilk normality test followed by a Kruskal-Wallis one-way ANOVA and Dunn's multiple comparisons tests were applied. n = number of patients quantified. **(F)** Representative microscopic images of PIWIL1 expression in TMA from CRC patients. Scale bar is 100 µm. **(G)** Kaplan-Meier survival analysis of cytoplasmic PIWIL1 expression in the cohort of CRC patients.

For box plots, the line is the median and the box represents the values included between the 25th and 75th percentiles. For other graphs, data represent the mean ± s.d. ns, not significant ($P > 0.05$); *$P < 0.05$, **$P < 0.01$, ***$P < 0.001$ and ****$P < 0.0001$. a.u., arbitrary units.

Figure 7: Aub mediates CRC-like intestinal hyperplasia in *Drosophila*.

(A, B) Representative confocal images of Aub staining (red) in the posterior midguts of control flies **(A)** or *Apc*^{1Q8} mutant flies **(B)** expressing GFP within ISCs/EBs (green). Dashed yellow squares delineate the high magnification shown in the right panels. **(C)** Quantification of Aub staining within ISCs/EBs in posterior midguts as in (A and B). Shapiro-Wilk normality test followed by Mann-Whitney t test were applied. n = number of cells quantified. 3 cells per gut/fly have been quantified and 10 flies per condition have been analysed. **(D)** Representative confocal images of MARCM clones (green) expressing a *LacZ* control transgene only (41 flies analysed) or in combination with *aub*^{RNAi} (33 flies analysed), and *Apc*^{1Q8} mutant clones only (35 flies analysed) or co-expressing *aub*^{RNAi} (38 flies analysed). Dashed white lines delineate the clonal margins. **(E)** Quantification of the number of cells in each MARCM clone of genotypes as in (D). Shapiro-Wilk normality test followed by Kruskal-Wallis one-way ANOVA and a Dunn's multiple comparisons tests were applied. n = number of clones quantified. **(F)** Quantification of PH3-positive cells in the posterior midguts of control flies expressing GFP alone; with *Wg::HA* or *aub*^{RNAi} or co-expressing *Wg::HA* and *aub*^{RNAi} within ISCs/EBs. A Shapiro-Wilk normality test followed by a Kruskal-Wallis one-way ANOVA and a Dunn's multiple comparisons tests were applied. n = number of midguts/flies quantified and are indicated below each graph in the same order of the genotypes and treatments presented in the graph. **(G, H)** Representative confocal images of Aub staining (red) in the posterior midguts of control flies expressing GFP only **(G)** or with the activated form of human *BRAF* (*Raf*^{GOF}) **(H)** within ISCs/EBs (green) for 2 days. Dashed yellow squares delineate the high magnification shown in the right panels. **(I)** Quantification of Aub staining within ISCs/EBs in posterior midguts as in (G and H). Shapiro-Wilk normality test followed by an unpaired t test were applied. n = number of cells quantified. 3 cells per gut/fly have been quantified and 10 flies per condition have been analysed. **(J, K)** Quantification of PH3-positive cells in the posterior midguts of control flies expressing GFP only; *Raf*^{GOF} or *Raf*^{GOF} and *aub*^{RNAi} within ISCs/EBs for 2 **(J)** or 3

days **(K)**, respectively. Shapiro-Wilk normality test followed by Kruskal-Wallis one-way ANOVA and Dunn's multiple comparisons tests were applied. n = number of midguts/flies quantified and are indicated below each graph in the same order of the genotypes and treatments presented in the graph. **(L)** Quantification of Dcp-1-positive cells in the lumen of midguts as in (Fig.S6D). Shapiro-Wilk normality test followed by one-way ANOVA and Sidak's multiple comparisons tests were applied. n = number of midguts/flies quantified and are indicated below each graph in the same order of the genotypes and treatments presented in the graph.

Data represent the mean ± s.d. ns, not significant ($P > 0.05$); *$P < 0.05$, **$P < 0.01$, ***$P < 0.001$ and ****$P < 0.0001$. a.u., arbitrary units. Nuclei are identified with DAPI. Scale bars are 50µm.

Figure S1: Aub regulates intestinal regeneration independently of piRNAs.

(A) Quantification of PH3-positive cells in the posterior midguts of flies fed with sucrose or *Pe* and expressing GFP only, with *piwi*^{RNAi} or *ago3*^{RNAi} within ISCs/EBs. n = number of midguts/flies quantified. **(B)** Representative confocal images of 7 or 14 days old MARCM clones (green) expressing a *LacZ* transgene only (4 and 9 flies analysed, respectively) or with *aub*^{RNAi} (5 and 8 flies analysed, respectively). Dashed white lines delineate clonal margins. **(C)** Quantification of the size of MARCM clones as in (B). n = number of clones quantified. **(D)** Quantification of PH3-positive cells in the posterior midguts of *w*^{1118} flies, *spnE*$^{\Delta 125}$/*spnE*$^{100-37}$; *vasa*^{PH165}/*vasa*^{D5} or *rhi*$^{18-5}$/*rhi*$^{18-7}$ flies fed with sucrose or *Pe*. n = number of midguts/flies quantified. **(E)** Quantification of PH3-positive cells in the posterior midguts of flies fed with sucrose or *Pe* and expressing GFP alone or with *vasa*^{RNAi}, *armi*^{RNAi} *or rhino*^{RNAi} within ISCs/EBs. n = number of midguts/flies quantified. **(F, G, H)** Representative confocal images of Aub staining (red) in the posterior midguts of flies expressing GFP alone **(F)**, with *piwi*^{RNAi} **(G)** or with *vasa*^{RNAi} **(H)** within ISCs (green) and fed with sucrose or *Pe*. Dashed yellow squares delineate the high magnification shown in the right panels. **(I)** Quantification of Aub staining within ISCs in the posterior midguts as in (F, G, H). n=number of cells quantified. 3 cells per gut/fly have been quantified and 10 flies per condition have been analysed.

In all cases, two-way ANOVA followed by Sidak's multiple comparisons test were used for statistical analysis. N are indicated below each graph in the same order of the genotypes and treatments presented in the graph.

Data represent the mean ± s.d. ns, not significant ($P > 0.05$); *$P < 0.05$, **$P < 0.01$, ***$P < 0.001$ and ****$P < 0.0001$. a.u., arbitrary units. Nuclei are identified with DAPI. Scale bars are 50µm.

Figure S2: Presence of piRNAs in the *Drosophila* midgut.

(A) Schematic representation of the *Drosophila* intestine. The green area highlights the portion of the intestine that was dissected for small RNA sequencing. **(B, B', C, C')** Size distribution (top graphs) of all transposon-mapping reads and the Uridine- and Adenine-frequencies of transposon-mapping reads of piRNA size (>22nt) (bottom graphs) in oxidized libraries from the whole intestine of control flies fed with sucrose or *Pe* **(B, B')** or in oxidized libraries from the whole intestine of *aub* mutant flies fed with sucrose or *Pe* **(C, C')**. siRNAs are typically sized at 21 or 22nt while piRNAs are longer than 22nt (see dashed black rectangles for higher magnification). Uridine (red) at the 1st base position of TE antisense piRNA reads (>22nt) is a common signature of all piRNAs while Adenine (green) at the 10th base position of TE sense piRNA reads is a signature of Ping-Pong piRNAs. **(D, E)** Quantification of TE antisense **(D)** and sense **(E)** piRNAs abundance as in (B, B', C, C'). Two-way ANOVA followed by a Sidak's multiple comparisons test were applied. n = 3 biological replicates.

Data represent the mean ± s.d. ns, not significant ($P > 0.05$); *$P < 0.05$, **$P < 0.01$, ***$P < 0.001$ and ****$P < 0.0001$. a.u., arbitrary units. TE, transposable elements; AS, antisense; S, sense.

Figure S3: Presence of piRNAs in the *Drosophila* intestine.

(A, B) Size distribution (top graphs) of all transposon-mapping reads and the Uridine- and Adenine-frequencies of transposon-mapping reads of piRNA size (>22nt) (bottom graphs) in oxidized libraries from control ovaries **(A)** or in unoxidized libraries from the whole intestine of control flies previously published (Siudeja et al., 2021) **(B)**. siRNAs are typically sized at 21 or 22nt while piRNAs are longer than 22nt (see dashed black rectangles for higher magnification). Uridine (red) at the 1st base position of TE antisense piRNA reads (>22nt) is a common signature of all piRNAs while Adenine (green) at the 10th base position of TE sense piRNA reads is a signature of Ping-Pong piRNAs. **(C-G)** Representation of the 0.5 kb tile analysis of piRNA abundance measurement in sorted ISCs/EBs from control flies fed with

sucrose or *Pe* **(C, D)** or from flies expressing *aub*^{RNAi} in ISCs/EBs and fed with sucrose or *Pe* **(E, F)** compared to ovaries. The same analysis was performed to compare piRNA abundance between ovaries from control flies and from flies expressing *aub*^{RNAi} in ISCs/EBs **(G)**. Tiles from piRNA clusters are coloured: cluster 38C in orange, cluster 42AB in blue and cluster flamenco in green. All other tiles are coloured in grey. a.u., arbitrary units. TE, transposable elements; AS, antisense; S, sense.

Figure S4: TE mRNA expression in ISCs/EBs and ovaries.

(A, B, C) Abundance of TE mRNAs in sorted control **(A)**; or *aub*^{RNAi} ISCs/EBs **(B)** from sucrose and *Pe* fed animals or from control and *aub*^{RNAi} ovaries obtained from a previously published study **(C)** (Senti et al., 2015). TE mRNA counts were normalised to one million transcript counts including host mRNAs (TPM). Red dashed lines indicate 4-fold changes in either direction. Red, blue and green represent TE mRNAs highly expressed in the gut, in the ovaries or in both tissues, respectively. **(D)** Schematic representation of the site-directed transgenesis induced to generate fly lines carrying inducible GFP tagged wild type Aub (*UAS-aub*^{WT}) or Aub mutant isoforms (*UAS-aub*^{AA} and *UAS-aub*^{ADH}). *UAS-aub*^{AA} contains a double point mutation in the PAZ domain (yellow), responsible for the loading of piRNAs, while *UAS-aub*^{ADH} carries a single mutation in the PIWI domain (red), responsible for Aub's endonuclease activity and essential for piRNA biogenesis. **(E)** Female fertility assays in *aub*^{HN2}/*aub*^{QC42} mutant flies without or with expression of *aub*^{WT}, *aub*^{AA} or *aub*^{ADH} in the germline. a.u., arbitrary units. TE, transposable elements.

Figure S5: Aub regulates protein translation of Sox21a and Myc.

(A, B, C) RT-qPCR for mRNA expression of *sox21a* **(A)***, myc* **(B)** *and socs36e* **(C)** in the whole adult *Drosophila* midgut relative to *rpl32* mRNA levels. n = 4 biological replicates with 30 midguts dissected for each replicate. Two-way ANOVA followed by a Sidak's multiple comparisons test were applied for statistical analysis. n = number of biological replicates and are indicated below each graph in the same order of the genotypes and treatments presented in the graph. **(D)** Representative confocal images of puromycin staining (red) in the posterior midguts of flies expressing *eIF3C*^{RNAi} within ISCs (green) and fed with sucrose or *Pe*. **(D')** Quantification of puromycin staining within ISCs in posterior midguts as in (Fig.4A-C and S5D). Two-

way ANOVA followed by Sidak's multiple comparisons test were applied. n = number of midguts/flies quantified and are indicated below each graph in the same order of the genotypes and treatments presented in the graph. **(E, F, G)** Representative confocal images of eIF3C staining (red) in the posterior midgut of flies expressing GFP alone **(E)**, with *myc*^{RNAi} **(F)** or *sox21a*^{RNAi} **(G)** within ISCs/EBs (green) and fed with sucrose or *Pe*. Quantification is shown in Fig.5K.

Data represent the mean±s.d. ns, not significant ($P>0.05$); *$P<0.05$, **$P<0.01$, ***$P<0.001$ and ****$P<0.0001$. a.u., arbitrary units. Nuclei are identified with DAPI. Scale bars are 50µm.

Figure S6: Aub role in intestinal tumourigenesis by MAPK signalling.

(A) Piwil1 expression in wild type and *Piwil1* mutant mouse testis. Dashed black squares delineate the high magnification shown in the right panels. **(B, C)** Quantification of PH3-positive cells in the posterior midguts of control flies expressing GFP alone or with *aub*^{RNAi} within ISCs/EBs. Flies were fed with sucrose or *Pe*. The quantification was performed after 2 (**B**) or 3 days (**C**) of RNAi induction. Two-way ANOVA followed by Sidak's multiple comparisons test were applied. n = number of midguts/flies quantified and are indicated below each graph in the same order of the genotypes and treatments presented in the graph. **(D)** Apical, basal and orthogonal confocal images of Dcp-1 staining (grey) to detect apoptosis in midguts overexpressing for 3 days GFP alone or with *Raf*^{GOF} in the absence or presence of *aub*^{RNAi}. Flies were fed with sucrose. Quantification is shown Fig.7L. (**E**) Quantification of Aub staining within ISCs/EBs in posterior midguts. A Shapiro-Wilk normality test followed by a Mann-Whitney t test were applied. n = number of cells quantified. 3 cells per gut/fly have been quantified and 15 flies per condition have been analysed. **(F, G)** Quantification of PH3-positive cells in the posterior midguts of flies expressing GFP alone; with *Ras*^{V12} or with *Ras*^{V12} and *aub*^{RNAi} within ISCs/EBs. Quantification was performed after 2 days **(F)** of 7 days **(G)** of RNAi co-expression with *Ras*^{V12}. Shapiro-Wilk normality test followed by a Kruskal-Wallis one-way ANOVA and Dunn's multiple comparisons tests were applied. n = number of midguts/flies quantified and are indicated below each graph in the same order of the genotypes and treatments presented in the graph.

Data represent the mean ± s.d. ns, not significant ($P > 0.05$); *$P < 0.05$, **$P < 0.01$, ***$P < 0.001$ and ****$P < 0.0001$. a.u., arbitrary units. Nuclei are identified with DAPI. Scale bars are 50µm.

References

AKBERGENOV, R., SI-AMMOUR, A., BLEVINS, T., AMIN, I., KUTTER, C., VANDERSCHUREN, H., ZHANG, P., GRUISSEM, W., MEINS, F., JR., HOHN, T. & POOGGIN, M. M. 2006. Molecular characterization of geminivirus-derived small RNAs in different plant species. *Nucleic Acids Res,* 34**,** 462-71.

ARAÚJO, T., KHAYAT, A., QUINTANA, L., CALCAGNO, D., MOURÃO, R., MODESTO, A., PAIVA, J., LIMA, A., MOREIRA, F., OLIVEIRA, E., SOUZA, M., OTHMAN, M., LIEHR, T., ABDELHAY, E., GOMES, R., SANTOS, S. & ASSUMPÇÃO, P. 2018. Piwi like RNA-mediated gene silencing 1 gene as a possible major player in gastric cancer. *World J Gastroenterol,* 24**,** 5338-5350.

ARAVIN, A., GAIDATZIS, D., PFEFFER, S., LAGOS-QUINTANA, M., LANDGRAF, P., IOVINO, N., MORRIS, P., BROWNSTEIN, M. J., KURAMOCHI-MIYAGAWA, S., NAKANO, T., CHIEN, M., RUSSO, J. J., JU, J., SHERIDAN, R., SANDER, C., ZAVOLAN, M. & TUSCHL, T. 2006. A novel class of small RNAs bind to MILI protein in mouse testes. *Nature,* 442**,** 203-207.

ARAVIN, A. A., HANNON, G. J. & BRENNECKE, J. 2007. The Piwi-piRNA Pathway Provides an Adaptive Defense in the Transposon Arms Race. *Science,* 318**,** 761-764.

ARAVIN, A. A., SACHIDANANDAM, R., GIRARD, A., FEJES-TOTH, K. & HANNON, G. J. 2007. Developmentally Regulated piRNA Clusters Implicate MILI in Transposon Control. *Science,* 316**,** 744-747.

ASANO, K., CLAYTON, J., SHALEV, A. & HINNEBUSCH, A. G. 2000. A multifactor complex of eukaryotic initiation factors, eIF1, eIF2, eIF3, eIF5, and initiator tRNA(Met) is an important translation initiation intermediate in vivo. *Genes Dev,* 14**,** 2534-46.

BANGI, E., MURGIA, C., TEAGUE, A. G., SANSOM, O. J. & CAGAN, R. L. 2016. Functional exploration of colorectal cancer genomes using Drosophila. *Nat Commun,* 7**,** 13615.

BARCKMANN, B., PIERSON, S., DUFOURT, J., PAPIN, C., ARMENISE, C., PORT, F., GRENTZINGER, T., CHAMBEYRON, S., BARONIAN, G., DESVIGNES, J.-P., CURK, T. & SIMONELIG, M. 2015. Aubergine iCLIP Reveals piRNA-Dependent Decay of mRNAs Involved in Germ Cell Development in the Early Embryo. *Cell Reports,* 12**,** 1205-1216.

BARTHA, Á. & GYŐRFFY, B. 2021. TNMplot.com: A Web Tool for the Comparison of Gene Expression in Normal, Tumor and Metastatic Tissues. *Int J Mol Sci,* 22.

BECALSKA, A. N., KIM, Y. R., BELLETIER, N. G., LERIT, D. A., SINSIMER, K. S. & GAVIS, E. R. 2011. Aubergine is a component of a nanos mRNA localization complex. *Dev Biol,* 349**,** 46-52.

BEEHLER-EVANS, R. & MICCHELLI, C. A. 2015. Generation of enteroendocrine cell diversity in midgut stem cell lineages. *Development,* 142**,** 654-64.

BITEAU, B. & JASPER, H. 2011. EGF signaling regulates the proliferation of intestinal stem cells in Drosophila. *Development,* 138**,** 1045-55.

BONFINI, A., DOBSON, A. J., DUNEAU, D., REVAH, J., LIU, X., HOUTZ, P. & BUCHON, N. 2021. Multiscale analysis reveals that diet-dependent midgut plasticity emerges from alterations in both stem cell niche coupling and enterocyte size. *Elife,* 10.

BRAND, A. H. & PERRIMON, N. 1994. Raf acts downstream of the EGF receptor to determine dorsoventral polarity during Drosophila oogenesis. *Genes Dev,* 8**,** 629-39.

BRENNECKE, J., ARAVIN, A. A., STARK, A., DUS, M., KELLIS, M., SACHIDANANDAM, R. & HANNON, G. J. 2007. Discrete Small RNA-Generating Loci as Master Regulators of Transposon Activity in Drosophila. *Cell,* 128**,** 1089-1103.

BROWER-TOLAND, B., FINDLEY, S. D., JIANG, L., LIU, L., YIN, H., DUS, M., ZHOU, P., ELGIN, S. C. & LIN, H. 2007. Drosophila PIWI associates with chromatin and interacts directly with HP1a. *Genes Dev,* 21**,** 2300-11.

BUCHON, N., BRODERICK, N. A., KURAISHI, T. & LEMAITRE, B. 2010. Drosophila EGFR pathway coordinates stem cell proliferation and gut remodeling following infection. *BMC Biol,* 8**,** 152.

BUCHON, N., OSMAN, D., DAVID, F. P., FANG, H. Y., BOQUETE, J. P., DEPLANCKE, B. & LEMAITRE, B. 2013. Morphological and molecular characterization of adult midgut compartmentalization in Drosophila. *Cell Rep,* 3**,** 1725-38.

CHEN, J., XU, N., WANG, C., HUANG, P., HUANG, H., JIN, Z., YU, Z., CAI, T., JIAO, R. & XI, R. 2018. Transient Scute activation via a self-stimulatory loop directs enteroendocrine cell pair specification from self-renewing intestinal stem cells. *Nat Cell Biol,* 20**,** 152-161.

CHEN, Z., CHE, Q., JIANG, F. Z., WANG, H. H., WANG, F. Y., LIAO, Y. & WAN, X. P. 2015. Piwil1 causes epigenetic alteration of PTEN gene via upregulation of DNA methyltransferase in type I endometrial cancer. *Biochem Biophys Res Commun,* 463**,** 876-80.

COOK, H. A., KOPPETSCH, B. S., WU, J. & THEURKAUF, W. E. 2004. The Drosophila SDE3 Homolog armitage Is Required for oskar mRNA Silencing and Embryonic Axis Specification. *Cell,* 116**,** 817-829.

CORDERO, J. B., STEFANATOS, R. K., MYANT, K., VIDAL, M. & SANSOM, O. J. 2012a. Non-autonomous crosstalk between the Jak/Stat and Egfr pathways mediates Apc1-driven intestinal stem cell hyperplasia in the Drosophila adult midgut. *Development,* 139**,** 4524-35.

CORDERO, J. B., STEFANATOS, R. K., SCOPELLITI, A., VIDAL, M. & SANSOM, O. J. 2012b. Inducible progenitor-derived Wingless regulates adult midgut regeneration in Drosophila. *The EMBO Journal,* 31**,** 3901-3917.

COX, D. N., CHAO, A., BAKER, J., CHANG, L., QIAO, D. & LIN, H. 1998. A novel class of evolutionarily conserved genes defined by piwi are essential for stem cell self-renewal. *Genes Dev,* 12**,** 3715-27.

COX, D. N., CHAO, A. & LIN, H. 2000. piwi encodes a nucleoplasmic factor whose activity modulates the number and division rate of germline stem cells. *Development,* 127**,** 503-514.

DAVID, A., DOLAN, B. P., HICKMAN, H. D., KNOWLTON, J. J., CLAVARINO, G., PIERRE, P., BENNINK, J. R. & YEWDELL, J. W. 2012. Nuclear translation visualized by ribosome-bound nascent chain puromycylation. *J Cell Biol,* 197**,** 45-57.

DELIU, L. P., GHOSH, A. & GREWAL, S. S. 2017. Investigation of protein synthesis in Drosophila larvae using puromycin labelling. *Biol Open,* 6**,** 1229-1234.

DUFOURT, J., BONTONOU, G., CHARTIER, A., JAHAN, C., MEUNIER, A.-C., PIERSON, S., HARRISON, P. F., PAPIN, C., BEILHARZ, T. H. & SIMONELIG, M. 2017. piRNAs and Aubergine cooperate with Wispy poly(A) polymerase to stabilize mRNAs in the germ plasm. *Nature Communications,* 8**,** 1305.

FUJII, K., ZHULYN, O., BYEON, G. W., GENUTH, N. R., KERR, C. H., WALSH, E. M. & BARNA, M. 2021. Controlling tissue patterning by translational regulation of signaling transcripts through the core translation factor eIF3c. *Dev Cell,* 56**,** 2928-2937.e9.

GENZOR, P., CORDTS, S. C., BOKIL, N. V. & HAASE, A. D. 2019. Aberrant expression of select piRNA-pathway genes does not reactivate piRNA silencing in cancer cells. *Proceedings of the National Academy of Sciences,* 116**,** 11111-11112.

GIRARD, A., SACHIDANANDAM, R., HANNON, G. J. & CARMELL, M. A. 2006. A germline-specific class of small RNAs binds mammalian Piwi proteins. *Nature,* 442**,** 199-202.

GUINNEY, J., DIENSTMANN, R., WANG, X., DE REYNIÈS, A., SCHLICKER, A., SONESON, C., MARISA, L., ROEPMAN, P., NYAMUNDANDA, G., ANGELINO, P., BOT, B. M., MORRIS, J. S., SIMON, I. M., GERSTER, S., FESSLER, E., DE SOUSA E MELO, F., MISSIAGLIA, E., RAMAY, H., BARRAS, D., HOMICSKO, K., MARU, D., MANYAM, G. C., BROOM, B., BOIGE, V., PEREZ-VILLAMIL, B., LADERAS, T., SALAZAR, R., GRAY, J. W., HANAHAN, D., TABERNERO, J., BERNARDS, R., FRIEND, S. H., LAURENT-PUIG, P., MEDEMA, J. P., SADANANDAM, A., WESSELS, L., DELORENZI, M., KOPETZ, S., VERMEULEN, L. & TEJPAR, S. 2015. The consensus molecular subtypes of colorectal cancer. *Nature Medicine,* 21**,** 1350-1356.

GUNAWARDANE, L. S., SAITO, K., NISHIDA, K. M., MIYOSHI, K., KAWAMURA, Y., NAGAMI, T., SIOMI, H. & SIOMI, M. C. 2007. A Slicer-Mediated Mechanism for Repeat-Associated siRNA 5' End Formation in Drosophila. *Science,* 315**,** 1587-1590.

1360 HAFNER, M., LANDGRAF, P., LUDWIG, J., RICE, A., OJO, T., LIN, C., HOLOCH, D., LIM, C. & TUSCHL, T.
1361 2008. Identification of microRNAs and other small regulatory RNAs using cDNA library
1362 sequencing. *Methods,* 44**,** 3-12.
1363 HAN, B. W., WANG, W., LI, C., WENG, Z. & ZAMORE, P. D. 2015. piRNA-guided transposon cleavage
1364 initiates Zucchini-dependent, phased piRNA production. *Science,* 348**,** 817-821.
1365 HARRIS, A. N. & MACDONALD, P. M. 2001. aubergine encodes a Drosophila polar granule component
1366 required for pole cell formation and related to eIF2C. *Development,* 128**,** 2823-2832.
1367 HOUWING, S., KAMMINGA, L. M., BEREZIKOV, E., CRONEMBOLD, D., GIRARD, A., VAN DEN ELST, H.,
1368 FILIPPOV, D. V., BLASER, H., RAZ, E., MOENS, C. B., PLASTERK, R. H., HANNON, G. J., DRAPER,
1369 B. W. & KETTING, R. F. 2007. A role for Piwi and piRNAs in germ cell maintenance and
1370 transposon silencing in Zebrafish. *Cell,* 129**,** 69-82.
1371 HUANG, H., YU, X., HAN, X., HAO, J., ZHAO, J., BEBEK, G., BAO, S., PRAYSON, R. A., KHALIL, A. M.,
1372 JANKOWSKY, E. & YU, J. S. 2021. Piwil1 Regulates Glioma Stem Cell Maintenance and
1373 Glioblastoma Progression. *Cell Reports,* 34**,** 108522.
1374 HUANG, XIAO A., YIN, H., SWEENEY, S., RAHA, D., SNYDER, M. & LIN, H. 2013. A Major Epigenetic
1375 Programming Mechanism Guided by piRNAs. *Developmental Cell,* 24**,** 502-516.
1376 IPSARO, J. J., HAASE, A. D., KNOTT, S. R., JOSHUA-TOR, L. & HANNON, G. J. 2012. The structural
1377 biochemistry of Zucchini implicates it as a nuclease in piRNA biogenesis. *Nature,* 491**,** 279-
1378 83.
1379 JANIC, A., MENDIZABAL, L., LLAMAZARES, S., ROSSELL, D. & GONZALEZ, C. 2010. Ectopic Expression
1380 of Germline Genes Drives Malignant Brain Tumor Growth in *Drosophila*. *Science,* 330**,** 1824-
1381 1827.
1382 JIANG, H., GRENLEY, M. O., BRAVO, M. J., BLUMHAGEN, R. Z. & EDGAR, B. A. 2011. EGFR/Ras/MAPK
1383 signaling mediates adult midgut epithelial homeostasis and regeneration in Drosophila. *Cell*
1384 *Stem Cell,* 8**,** 84-95.
1385 JIANG, H., PATEL, P. H., KOHLMAIER, A., GRENLEY, M. O., MCEWEN, D. G. & EDGAR, B. A. 2009.
1386 Cytokine/Jak/Stat Signaling Mediates Regeneration and Homeostasis in the Drosophila
1387 Midgut. *Cell,* 137**,** 1343-1355.
1388 JIVOTOVSKAYA, A. V., VALÁSEK, L., HINNEBUSCH, A. G. & NIELSEN, K. H. 2006. Eukaryotic translation
1389 initiation factor 3 (eIF3) and eIF2 can promote mRNA binding to 40S subunits independently
1390 of eIF4G in yeast. *Mol Cell Biol,* 26**,** 1355-72.
1391 JONES, B. C., WOOD, J. G., CHANG, C., TAM, A. D., FRANKLIN, M. J., SIEGEL, E. R. & HELFAND, S. L.
1392 2016. A somatic piRNA pathway in the Drosophila fat body ensures metabolic homeostasis
1393 and normal lifespan. *Nat Commun,* 7**,** 13856.
1394 KIRINO, Y. & MOURELATOS, Z. 2007. Mouse Piwi-interacting RNAs are 2'-O-methylated at their 3'
1395 termini. *Nat Struct Mol Biol,* 14**,** 347-8.
1396 KNIGHT, J. R. P., ALEXANDROU, C., SKALKA, G. L., VLAHOV, N., PENNEL, K., OFFICER, L., TEODOSIO, A.,
1397 KANELLOS, G., GAY, D. M., MAY-WILSON, S., SMITH, E. M., NAJUMUDEEN, A. K., GILROY, K.,
1398 RIDGWAY, R. A., FLANAGAN, D. J., SMITH, R. C. L., MCDONALD, L., MACKAY, C., CHEASTY, A.,
1399 MCARTHUR, K., STANWAY, E., LEACH, J. D., JACKSTADT, R., WALDRON, J. A., CAMPBELL, A.
1400 D., VLACHOGIANNIS, G., VALERI, N., HAIGIS, K. M., SONENBERG, N., PROUD, C. G., JONES, N.
1401 P., SWARBRICK, M. E., MCKINNON, H. J., FALLER, W. J., LE QUESNE, J., EDWARDS, J., WILLIS,
1402 A. E., BUSHELL, M. & SANSOM, O. J. 2021. MNK Inhibition Sensitizes KRAS-Mutant Colorectal
1403 Cancer to mTORC1 Inhibition by Reducing eIF4E Phosphorylation and c-MYC Expression.
1404 *Cancer Discov,* 11**,** 1228-1247.
1405 KORZELIUS, J., AZAMI, S., RONNEN-ORON, T., KOCH, P., BALDAUF, M., MEIER, E., RODRIGUEZ-
1406 FERNANDEZ, I. A., GROTH, M., SOUSA-VICTOR, P. & JASPER, H. 2019. The WT1-like
1407 transcription factor Klumpfuss maintains lineage commitment of enterocyte progenitors in
1408 the Drosophila intestine. *Nature Communications,* 10**,** 4123.

1409 KRISHNAN, P., GHOSH, S., GRAHAM, K., MACKEY, J. R., KOVALCHUK, O. & DAMARAJU, S. 2016. Piwi-
1410 interacting RNAs and PIWI genes as novel prognostic markers for breast cancer. *Oncotarget,*
1411 7.
1412 LEE, T. & LUO, L. 1999. Mosaic analysis with a repressible cell marker for studies of gene function in
1413 neuronal morphogenesis. *Neuron,* 22**,** 451-61.
1414 LEE, W. C., BEEBE, K., SUDMEIER, L. & MICCHELLI, C. A. 2009. Adenomatous polyposis coli regulates
1415 Drosophila intestinal stem cell proliferation. *Development,* 136**,** 2255-64.
1416 LI, C., VAGIN, V. V., LEE, S., XU, J., MA, S., XI, H., SEITZ, H., HORWICH, M. D., SYRZYCKA, M., HONDA,
1417 B. M., KITTLER, E. L. W., ZAPP, M. L., KLATTENHOFF, C., SCHULZ, N., THEURKAUF, W. E.,
1418 WENG, Z. & ZAMORE, P. D. 2009. Collapse of Germline piRNAs in the Absence of Argonaute3
1419 Reveals Somatic piRNAs in Flies. *Cell,* 137**,** 509-521.
1420 LI, F., YUAN, P., RAO, M., JIN, C.-H., TANG, W., RONG, Y.-F., HU, Y.-P., ZHANG, F., WEI, T., YIN, Q.,
1421 LIANG, T., WU, L., LI, J., LI, D., LIU, Y., LOU, W., ZHAO, S. & LIU, M.-F. 2020. piRNA-
1422 independent function of PIWIL1 as a co-activator for anaphase promoting
1423 complex/cyclosome to drive pancreatic cancer metastasis. *Nature Cell Biology,* 22**,** 425-438.
1424 LI, W., MARTINEZ-USEROS, J., GARCIA-CARBONERO, N., FERNANDEZ-ACEÑERO, M. J., ORTEGA-
1425 MEDINA, L., GARCIA-BOTELLA, S., PEREZ-AGUIRRE, E., DIEZ-VALLADARES, L. & GARCIA-
1426 FONCILLAS, J. 2019. The Prognosis Value of PIWIL1 and PIWIL2 Expression in Pancreatic
1427 Cancer. *J Clin Med,* 8.
1428 LIN, G., XU, N. & XI, R. 2008. Paracrine Wingless signalling controls self-renewal of Drosophila
1429 intestinal stem cells. *Nature,* 455**,** 1119-1123.
1430 LIN, G., XU, N. & XI, R. 2010. Paracrine unpaired signaling through the JAK/STAT pathway controls
1431 self-renewal and lineage differentiation of drosophila intestinal stem cells. *J Mol Cell Biol,* 2**,**
1432 37-49.
1433 LIN, H. & SPRADLING, A. C. 1997. A novel group of pumilio mutations affects the asymmetric division
1434 of germline stem cells in the Drosophila ovary. *Development,* 124**,** 2463-76.
1435 LIN, Y., ZHENG, J. & LIN, D. 2021. PIWI-interacting RNAs in human cancer. *Seminars in Cancer*
1436 *Biology,* 75**,** 15-28.
1437 LIU, T., WANG, J., SUN, L., LI, M., HE, X., JIANG, J. & ZHOU, Q. 2021. Piwi-interacting RNA-651
1438 promotes cell proliferation and migration and inhibits apoptosis in breast cancer by
1439 facilitating DNMT1-mediated PTEN promoter methylation. *Cell Cycle,* 20**,** 1603-1616.
1440 MA, X., ZHU, X., HAN, Y., STORY, B., DO, T., SONG, X., WANG, S., ZHANG, Y., BLANCHETTE, M.,
1441 GOGOL, M., HALL, K., PEAK, A., ANOJA, P. & XIE, T. 2017. Aubergine Controls Germline Stem
1442 Cell Self-Renewal and Progeny Differentiation via Distinct Mechanisms. *Developmental Cell,*
1443 41**,** 157-169.e5.
1444 MAJUMDAR, R., BANDYOPADHYAY, A. & MAITRA, U. 2003. Mammalian Translation Initiation Factor
1445 eIF1 Functions with eIF1A and eIF3 in the Formation of a Stable 40 S Preinitiation Complex*.
1446 *Journal of Biological Chemistry,* 278**,** 6580-6587.
1447 MALONE, C. D., BRENNECKE, J., DUS, M., STARK, A., MCCOMBIE, W. R., SACHIDANANDAM, R. &
1448 HANNON, G. J. 2009. Specialized piRNA Pathways Act in Germline and Somatic Tissues of the
1449 Drosophila Ovary. *Cell,* 137**,** 522-535.
1450 MARIANES, A. & SPRADLING, A. C. 2013. Physiological and stem cell compartmentalization within the
1451 Drosophila midgut. *Elife,* 2**,** e00886.
1452 MARKSTEIN, M., DETTORRE, S., CHO, J., NEUMÜLLER, R. A., CRAIG-MÜLLER, S. & PERRIMON, N.
1453 2014. Systematic screen of chemotherapeutics in Drosophila stem cell tumors. *Proc Natl*
1454 *Acad Sci U S A,* 111**,** 4530-5.
1455 MARTINEZ, V. D., ENFIELD, K. S. S., ROWBOTHAM, D. A. & LAM, W. L. 2016. An atlas of gastric PIWI-
1456 interacting RNA transcriptomes and their utility for identifying signatures of gastric cancer
1457 recurrence. *Gastric Cancer,* 19**,** 660-665.
1458 MARTINEZ, V. D., VUCIC, E. A., THU, K. L., HUBAUX, R., ENFIELD, K. S. S., PIKOR, L. A., BECKER-
1459 SANTOS, D. D., BROWN, C. J., LAM, S. & LAM, W. L. 2015. Unique somatic and malignant

expression patterns implicate PIWI-interacting RNAs in cancer-type specific biology. *Scientific Reports,* 5**,** 10423.
MENG, FANJU W. & BITEAU, B. 2015. A Sox Transcription Factor Is a Critical Regulator of Adult Stem Cell Proliferation in the Drosophila Intestine. *Cell Reports,* 13**,** 906-914.
MICCHELLI, C. A. & PERRIMON, N. 2006. Evidence that stem cells reside in the adult Drosophila midgut epithelium. *Nature,* 439**,** 475-9.
MOCHIZUKI, K., FINE, N. A., FUJISAWA, T. & GOROVSKY, M. A. 2002. Analysis of a piwi-related gene implicates small RNAs in genome rearrangement in tetrahymena. *Cell,* 110**,** 689-99.
NISHIMASU, H., ISHIZU, H., SAITO, K., FUKUHARA, S., KAMATANI, M. K., BONNEFOND, L., MATSUMOTO, N., NISHIZAWA, T., NAKANAGA, K., AOKI, J., ISHITANI, R., SIOMI, H., SIOMI, M. C. & NUREKI, O. 2012. Structure and function of Zucchini endoribonuclease in piRNA biogenesis. *Nature,* 491**,** 284-7.
OBATA, F., TSUDA-SAKURAI, K., YAMAZAKI, T., NISHIO, R., NISHIMURA, K., KIMURA, M., FUNAKOSHI, M. & MIURA, M. 2018. Nutritional Control of Stem Cell Division through S-Adenosylmethionine in Drosophila Intestine. *Developmental Cell,* 44**,** 741-751.e3.
OHARA, T., SAKAGUCHI, Y., SUZUKI, T., UEDA, H., MIYAUCHI, K. & SUZUKI, T. 2007. The 3' termini of mouse Piwi-interacting RNAs are 2'-O-methylated. *Nat Struct Mol Biol,* 14**,** 349-50.
OHLSTEIN, B. & SPRADLING, A. 2006. The adult Drosophila posterior midgut is maintained by pluripotent stem cells. *Nature,* 439**,** 470-4.
PAL-BHADRA, M., LEIBOVITCH, B. A., GANDHI, S. G., RAO, M., BHADRA, U., BIRCHLER, J. A. & ELGIN, S. C. R. 2004. Heterochromatic Silencing and HP1 Localization in *Drosophila* Are Dependent on the RNAi Machinery. *Science,* 303**,** 669-672.
PANE, A., WEHR, K. & SCHÜPBACH, T. 2007. zucchini and squash encode two putative nucleases required for rasiRNA production in the Drosophila germline. *Dev Cell,* 12**,** 851-62.
PEROCHON, J., YU, Y., AUGHEY, G. N., MEDINA, A. B., SOUTHALL, T. D. & CORDERO, J. B. 2021. Dynamic adult tracheal plasticity drives stem cell adaptation to changes in intestinal homeostasis in Drosophila. *Nat Cell Biol,* 23**,** 485-496.
PETSAKOU, A. & PERRIMON, N. 2023. Bioelectric regulation of intestinal stem cells. *Trends Cell Biol,* 33**,** 555-567.
QIAO, D., ZEEMAN, A. M., DENG, W., LOOIJENGA, L. H. & LIN, H. 2002. Molecular characterization of hiwi, a human member of the piwi gene family whose overexpression is correlated to seminomas. *Oncogene,* 21**,** 3988-99.
RAJASETHUPATHY, P., ANTONOV, I., SHERIDAN, R., FREY, S., SANDER, C., TUSCHL, T. & KANDEL, ERIC R. 2012. A Role for Neuronal piRNAs in the Epigenetic Control of Memory-Related Synaptic Plasticity. *Cell,* 149**,** 693-707.
RAMAT, A., GARCIA-SILVA, M.-R., JAHAN, C., NAÏT-SAÏDI, R., DUFOURT, J., GARRET, C., CHARTIER, A., CREMASCHI, J., PATEL, V., DECOURCELLE, M., BASTIDE, A., JUGE, F. & SIMONELIG, M. 2020. The PIWI protein Aubergine recruits eIF3 to activate translation in the germ plasm. *Cell Research,* 30**,** 421-435.
RODE, S., OHM, H., ANHÄUSER, L., WAGNER, M., ROSING, M., DENG, X., SIN, O., LEIDEL, S. A., STORKEBAUM, E., RENTMEISTER, A., ZHU, S. & RUMPF, S. 2018. Differential Requirement for Translation Initiation Factor Pathways during Ecdysone-Dependent Neuronal Remodeling in Drosophila. *Cell Rep,* 24**,** 2287-2299.e4.
ROJAS-RÍOS, P., CHARTIER, A., ENJOLRAS, C., CREMASCHI, J., GARRET, C., BOUGHLITA, A., RAMAT, A. & SIMONELIG, M. 2023. piRNAs are regulators of metabolic reprogramming in stem cells. *bioRxiv***,** 2023.10.31.564965.
ROJAS-RÍOS, P., CHARTIER, A., PIERSON, S. & SIMONELIG, M. 2017. Aubergine and piRNAs promote germline stem cell self-renewal by repressing the proto-oncogene Cbl. *The EMBO Journal,* 36**,** 3194-3211.
ROSS, R. J., WEINER, M. M. & LIN, H. 2014. PIWI proteins and PIWI-interacting RNAs in the soma. *Nature,* 505**,** 353-359.

1511 ROUGET, C., PAPIN, C., BOUREUX, A., MEUNIER, A.-C., FRANCO, B., ROBINE, N., LAI, E. C., PELISSON,
1512 A. & SIMONELIG, M. 2010. Maternal mRNA deadenylation and decay by the piRNA pathway
1513 in the early Drosophila embryo. *Nature,* 467**,** 1128-1132.
1514 SAHIN, H. B., KARATAS, O. F., SPECCHIA, V., TOMMASO, S. D., DIEBOLD, C., BOZZETTI, M. P. &
1515 GIANGRANDE, A. 2016. Novel mutants of the aubergine gene. *Fly (Austin),* 10**,** 81-90.
1516 SAITO, K., NISHIDA, K. M., MORI, T., KAWAMURA, Y., MIYOSHI, K., NAGAMI, T., SIOMI, H. & SIOMI,
1517 M. C. 2006. Specific association of Piwi with rasiRNAs derived from retrotransposon and
1518 heterochromatic regions in the Drosophila genome. *Genes Dev,* 20**,** 2214-22.
1519 SAITO, K., SAKAGUCHI, Y., SUZUKI, T., SUZUKI, T., SIOMI, H. & SIOMI, M. C. 2007. Pimet, the
1520 Drosophila homolog of HEN1, mediates 2'-O-methylation of Piwi- interacting RNAs at their 3'
1521 ends. *Genes Dev,* 21**,** 1603-8.
1522 SCHATOFF, E. M., LEACH, B. I. & DOW, L. E. 2017. WNT Signaling and Colorectal Cancer. *Current*
1523 *Colorectal Cancer Reports,* 13**,** 101-110.
1524 SCHÜPBACH, T. & WIESCHAUS, E. 1989. Female sterile mutations on the second chromosome of
1525 Drosophila melanogaster. I. Maternal effect mutations. *Genetics,* 121**,** 101-17.
1526 SCHÜPBACH, T. & WIESCHAUS, E. 1991. Female sterile mutations on the second chromosome of
1527 Drosophila melanogaster. II. Mutations blocking oogenesis or altering egg morphology.
1528 *Genetics,* 129**,** 1119-36.
1529 SEGDITSAS, S. & TOMLINSON, I. 2006. Colorectal cancer and genetic alterations in the Wnt pathway.
1530 *Oncogene,* 25**,** 7531-7.
1531 SELLITTO, A., GELES, K., D'AGOSTINO, Y., CONTE, M., ALEXANDROVA, E., ROCCO, D., NASSA, G.,
1532 GIURATO, G., TARALLO, R., WEISZ, A. & RIZZO, F. 2019. Molecular and Functional
1533 Characterization of the Somatic PIWIL1/piRNA Pathway in Colorectal Cancer Cells. *Cells,* 8**,**
1534 1390.
1535 SENTI, K. A., JURCZAK, D., SACHIDANANDAM, R. & BRENNECKE, J. 2015. piRNA-guided slicing of
1536 transposon transcripts enforces their transcriptional silencing via specifying the nuclear
1537 piRNA repertoire. *Genes Dev,* 29**,** 1747-62.
1538 SHARMA, A. K., NELSON, M. C., BRANDT, J. E., WESSMAN, M., MAHMUD, N., WELLER, K. P. &
1539 HOFFMAN, R. 2001. Human CD34+ stem cells express the hiwigene, a human homologue of
1540 the Drosophila genepiwi. *Blood,* 97**,** 426-434.
1541 SHI, S., YANG, Z.-Z., LIU, S., YANG, F. & LIN, H. 2020. PIWIL1 promotes gastric cancer via a piRNA-
1542 independent mechanism. *Proceedings of the National Academy of Sciences,* 117**,** 22390-
1543 22401.
1544 SIDDIQI, S., TERRY, M. & MATUSHANSKY, I. 2012. Hiwi mediated tumorigenesis is associated with
1545 DNA hypermethylation. *PLoS One,* 7**,** e33711.
1546 SIENSKI, G., BATKI, J., SENTI, K. A., DÖNERTAS, D., TIRIAN, L., MEIXNER, K. & BRENNECKE, J. 2015.
1547 Silencio/CG9754 connects the Piwi-piRNA complex to the cellular heterochromatin
1548 machinery. *Genes Dev,* 29**,** 2258-71.
1549 SIOMI, M. C., SATO, K., PEZIC, D. & ARAVIN, A. A. 2011. PIWI-interacting small RNAs: the vanguard of
1550 genome defence. *Nature Reviews Molecular Cell Biology,* 12**,** 246-258.
1551 SIUDEJA, K., VAN DEN BEEK, M., RIDDIFORD, N., BOUMARD, B., WURMSER, A., STEFANUTTI, M.,
1552 LAMEIRAS, S. & BARDIN, A. J. 2021. Unraveling the features of somatic transposition in the
1553 Drosophila intestine. *Embo j,* 40**,** e106388.
1554 SONG, P., YANG, F., JIN, H. & WANG, X. 2021. The regulation of protein translation and its
1555 implications for cancer. *Signal Transduction and Targeted Therapy,* 6**,** 68.
1556 SOUSA-VICTOR, P., AYYAZ, A., HAYASHI, R., QI, Y., MADDEN, D. T., LUNYAK, V. V. & JASPER, H. 2017.
1557 Piwi Is Required to Limit Exhaustion of Aging Somatic Stem Cells. *Cell reports,* 20**,** 2527-2537.
1558 SUN, R., GAO, C.-L., LI, D.-H., LI, B.-J. & DING, Y.-H. 2017. Expression Status of PIWIL1 as a Prognostic
1559 Marker of Colorectal Cancer. *Disease Markers,* 2017**,** 1204937.
1560 TAMAMOUNA, V., RAHMAN, M. M., PETERSSON, M., CHARALAMBOUS, I., KUX, K., MAINOR, H.,
1561 BOLENDER, V., ISBILIR, B., EDGAR, B. A. & PITSOULI, C. 2021. Remodelling of oxygen-

transporting tracheoles drives intestinal regeneration and tumorigenesis in Drosophila. *Nat Cell Biol,* 23**,** 497-510.
TANG, X., LIU, N., QI, H. & LIN, H. 2023. Piwi maintains homeostasis in the Drosophila adult intestine. *Stem Cell Reports,* 18**,** 503-518.
TOSAR, J. P., GARCÍA-SILVA, M. R. & CAYOTA, A. 2021. Circulating SNORD57 rather than piR-54265 is a promising biomarker for colorectal cancer: common pitfalls in the study of somatic piRNAs in cancer. *Rna,* 27**,** 403-410.
VAGIN, V. V., SIGOVA, A., LI, C., SEITZ, H., GVOZDEV, V. & ZAMORE, P. D. 2006. A distinct small RNA pathway silences selfish genetic elements in the germline. *Science,* 313**,** 320-4.
VALÁSEK, L., MATHEW, A. A., SHIN, B. S., NIELSEN, K. H., SZAMECZ, B. & HINNEBUSCH, A. G. 2003. The yeast eIF3 subunits TIF32/a, NIP1/c, and eIF5 make critical connections with the 40S ribosome in vivo. *Genes Dev,* 17**,** 786-99.
VOUREKAS, A., ALEXIOU, P., VRETTOS, N., MARAGKAKIS, M. & MOURELATOS, Z. 2016. Sequence-dependent but not sequence-specific piRNA adhesion traps mRNAs to the germ plasm. *Nature,* 531**,** 390-394.
WAJED, S. A., LAIRD, P. W. & DEMEESTER, T. R. 2001. DNA methylation: an alternative pathway to cancer. *Ann Surg,* 234**,** 10-20.
WALDRON, J. A., KANELLOS, G., SMITH, R. C. L., KNIGHT, J. R. P., MUNRO, J., ALEXANDROU, C., VLAHOV, N., PARDO-FERNANDEZ, L., MOORE, M., GILLEN, S. L., STRATHDEE, D., STEVENSON, D., WARRANDER, F. C., GILROY, K., NIXON, C., CADDEN, B., POWLEY, I., OFFICER-JONES, L., BALLANTYNE, F., HAY, J., PENNEL, K., EDWARDS, J., CAMPBELL, A. D., RIDGWAY, R. A., COFFELT, S. B., NORMAN, J., QUESNE, J. L., BUSHELL, M. & SANSOM, O. J. 2023. eIF4A1 is essential for reprogramming the translational landscape of Wnt-driven colorectal cancers. *bioRxiv***,** 2023.11.10.566546.
WANG, H.-L., CHEN, B.-B., CAO, X.-G., WANG, J., HU, X.-F., MU, X.-Q. & CHEN, X.-B. 2015a. The clinical significances of the abnormal expressions of Piwil1 and Piwil2 in colonic adenoma and adenocarcinoma. *OncoTargets and Therapy,* 8**,** 1259-1264.
WANG, L., ZENG, X., RYOO, H. D. & JASPER, H. 2014. Integration of UPRER and Oxidative Stress Signaling in the Control of Intestinal Stem Cell Proliferation. *PLOS Genetics,* 10**,** e1004568.
WANG, N., TAN, H.-Y., LU, Y., CHAN, Y.-T., WANG, D., GUO, W., XU, Y., ZHANG, C., CHEN, F., TANG, G. & FENG, Y. 2021. PIWIL1 governs the crosstalk of cancer cell metabolism and immunosuppressive microenvironment in hepatocellular carcinoma. *Signal Transduction and Targeted Therapy,* 6**,** 86.
WANG, W., HAN, B. W., TIPPING, C., GE, D. T., ZHANG, Z., WENG, Z. & ZAMORE, P. D. 2015b. Slicing and Binding by Ago3 or Aub Trigger Piwi-Bound piRNA Production by Distinct Mechanisms. *Mol Cell,* 59**,** 819-30.
WANG, X., JIANG, C., FU, B., ZHU, R., DIAO, F., XU, N., CHEN, Z., TAO, W. & LI, C. J. 2015c. MILI, a PIWI family protein, inhibits melanoma cell migration through methylation of LINE1. *Biochem Biophys Res Commun,* 457**,** 514-9.
WANG, Y., JIANG, Y., MA, N., SANG, B., HU, X., CONG, X. & LIU, Z. 2015d. Overexpression of Hiwi Inhibits the Growth and Migration of Chronic Myeloid Leukemia Cells. *Cell Biochem Biophys,* 73**,** 117-24.
WANG, Z., LIU, N., SHI, S., LIU, S. & LIN, H. 2016. The Role of PIWIL4, an Argonaute Family Protein, in Breast Cancer*. *Journal of Biological Chemistry,* 291**,** 10646-10658.
WENG, W., LIU, N., TOIYAMA, Y., KUSUNOKI, M., NAGASAKA, T., FUJIWARA, T., WEI, Q., QIN, H., LIN, H., MA, Y. & GOEL, A. 2018. Novel evidence for a PIWI-interacting RNA (piRNA) as an oncogenic mediator of disease progression, and a potential prognostic biomarker in colorectal cancer. *Mol Cancer,* 17**,** 16.
WIEGERING, A., UTHE, F. W., JAMIESON, T., RUOSS, Y., HÜTTENRAUCH, M., KÜSPERT, M., PFANN, C., NIXON, C., HEROLD, S., WALZ, S., TARANETS, L., GERMER, C. T., ROSENWALD, A., SANSOM,

O. J. & EILERS, M. 2015. Targeting Translation Initiation Bypasses Signaling Crosstalk Mechanisms That Maintain High MYC Levels in Colorectal Cancer. *Cancer Discov,* 5**,** 768-781.

WILSON, J. E., CONNELL, J. E. & MACDONALD, P. M. 1996. aubergine enhances oskar translation in the Drosophila ovary. *Development,* 122**,** 1631-9.

XIE, K., ZHANG, K., KONG, J., WANG, C., GU, Y., LIANG, C., JIANG, T., QIN, N., LIU, J., GUO, X., HUO, R., LIU, M., MA, H., DAI, J. & HU, Z. 2018. Cancer-testis gene PIWIL1 promotes cell proliferation, migration, and invasion in lung adenocarcinoma. *Cancer Medicine,* 7**,** 157-166.

XU, N., WANG, S. Q., TAN, D., GAO, Y., LIN, G. & XI, R. 2011. EGFR, Wingless and JAK/STAT signaling cooperatively maintain Drosophila intestinal stem cells. *Dev Biol,* 354**,** 31-43.

YAJIMA, M. & WESSEL, G. M. 2011. The multiple hats of Vasa: its functions in the germline and in cell cycle progression. *Mol Reprod Dev,* 78**,** 861-7.

YIN, J., QI, W., JI, C. G., ZHANG, D. X., XIE, X. L., DING, Q., JIANG, X. Y., HAN, J. & JIANG, H. Q. 2019. Small RNA sequencing revealed aberrant piRNA expression profiles in colorectal cancer. *Oncol Rep,* 42**,** 263-272.

ZENG, X., CHAUHAN, C. & HOU, S. X. 2010. Characterization of midgut stem cell- and enteroblast-specific Gal4 lines in drosophila. *Genesis (New York, N.Y. : 2000),* 48**,** 607-611.

ZENG, X. & HOU, S. X. 2015. Enteroendocrine cells are generated from stem cells through a distinct progenitor in the adult Drosophila posterior midgut. *Development,* 142**,** 644-53.

ZHANG, H., REN, Y., XU, H., PANG, D., DUAN, C. & LIU, C. 2013. The expression of stem cell protein Piwil2 and piR-932 in breast cancer. *Surgical Oncology,* 22**,** 217-223.

ZHOU, F., RASMUSSEN, A., LEE, S. & AGAISSE, H. 2013. The UPD3 cytokine couples environmental challenge and intestinal stem cell division through modulation of JAK/STAT signaling in the stem cell microenvironment. *Dev Biol,* 373**,** 383-93.

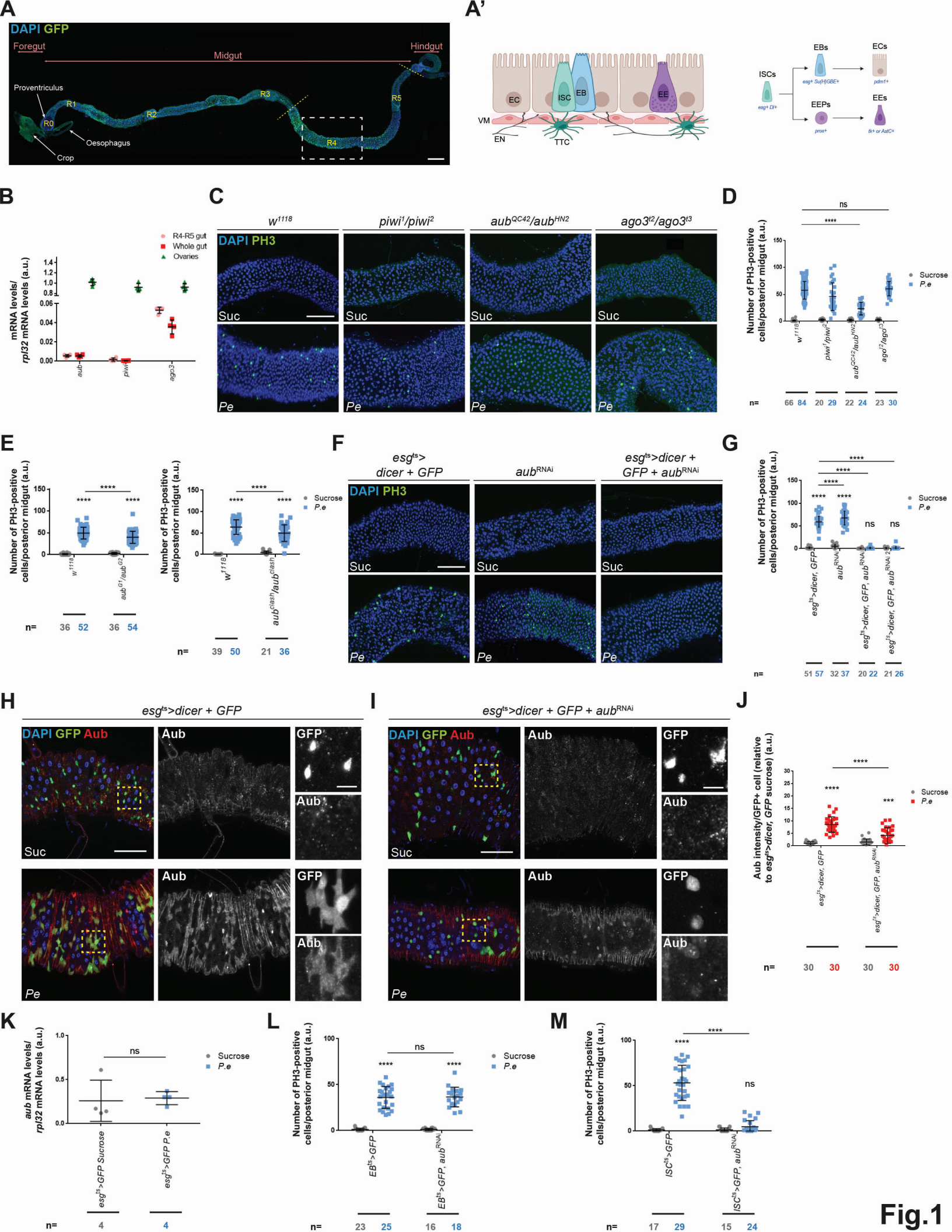
A
DAPI GFP
Foregut
Midgut
Hindgut
Proventriculus
R0
R1
R2
R3
R4
R5
Oesophagus
Crop
A'
EC
ISC
EB
EE
VM
EN
TTC
ISCs
EBs
ECs
EEPs
EEs
B
mRNA levels/ rpl32 mRNA levels (a.u.)
R4-R5 gut
Whole gut
Ovaries
aub
piwi
ago3
C
w1118
piwi1/piwi2
aubQC42/aubHN2
ago3t2/ago3t3
DAPI PH3
Suc
Pe
D
Number of PH3-positive cells/posterior midgut (a.u.)
ns
****
Sucrose
P.e
n=
66 84 20 29 22 24 23 30
E
Number of PH3-positive cells/posterior midgut (a.u.)
w1118
aubG1/aubG2
aubclash/aubclash
n=
36 52 36 54
39 50 21 36
F
esgts> dicer + GFP
aubRNAi
esgts>dicer + GFP + aubRNAi
DAPI PH3
Suc
Pe
G
Number of PH3-positive cells/posterior midgut (a.u.)
esgts>dicer, GFP
aubRNAi
esgts>dicer, GFP, aubRNAi
esgts>dicer, GFP, aubRNAi 2
n=
51 57 32 37 20 22 21 26
H
esgts>dicer + GFP
DAPI GFP Aub
Aub
GFP
Suc
Pe
I
esgts>dicer + GFP + aubRNAi
J
Aub intensity/GFP+ cell (relative to esgts>dicer, GFP sucrose) (a.u.)
***
n=
30 30 30 30
K
aub mRNA levels/ rpl32 mRNA levels (a.u.)
esgts>GFP Sucrose
esgts>GFP P.e
n=
4 4
L
Number of PH3-positive cells/posterior midgut (a.u.)
EBts>GFP
EBts>GFP, aubRNAi
n=
23 25 16 18
M
Number of PH3-positive cells/posterior midgut (a.u.)
ISCts>GFP
ISCts>GFP, aubRNAi
n=
17 29 15 24
Fig.1

Fig.2

A

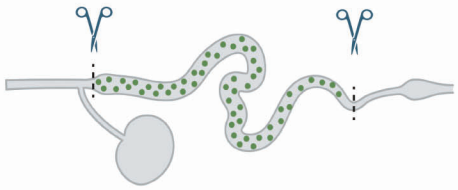

B

Oxidized library (rep #2)
esg^{ts}>*GFP* Sucrose

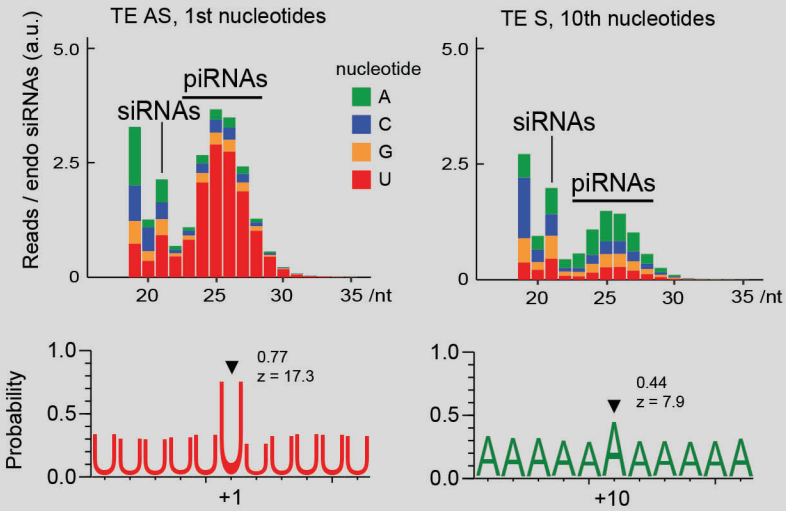

B'

Oxidized library (rep #3)
esg^{ts}>*GFP Pe*

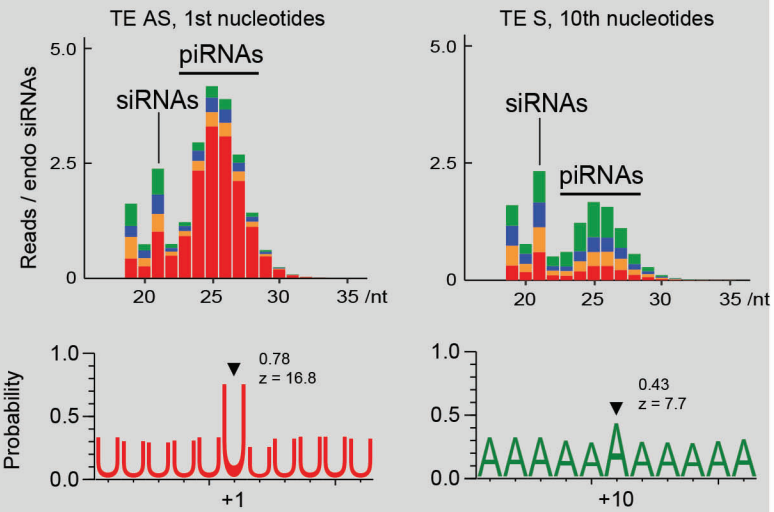

C

Oxidized library (rep #1)
esg^{ts}>*GFP + aub*^{RNAi} Sucrose

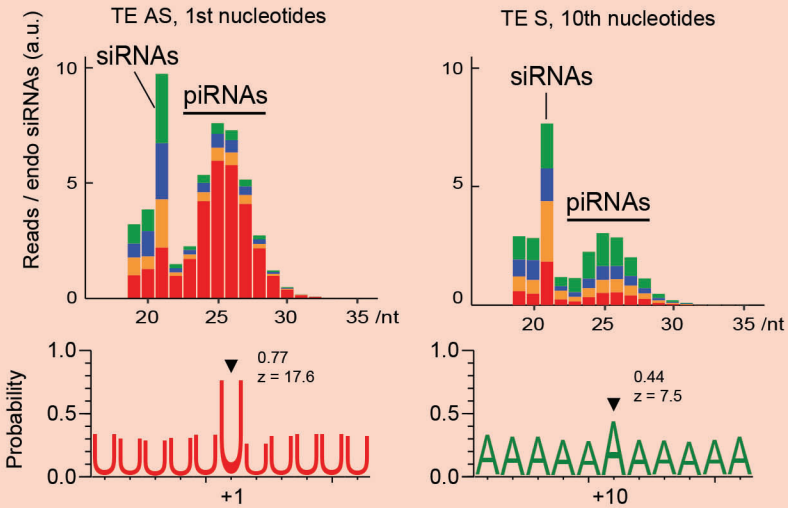

C'

Oxidized library (rep #1)
esg^{ts}>*GFP + aub*^{RNAi} *Pe*

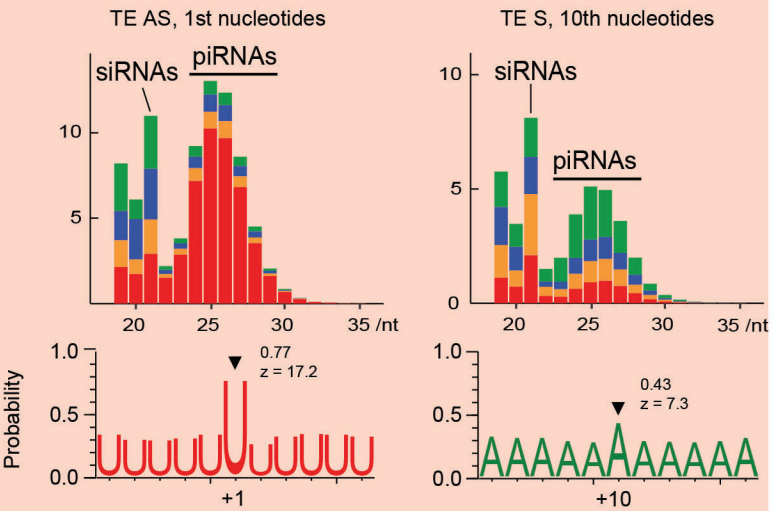

D

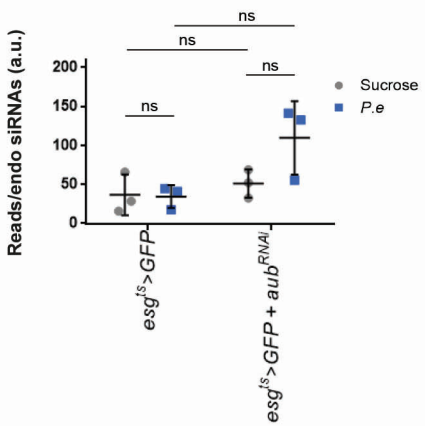

E

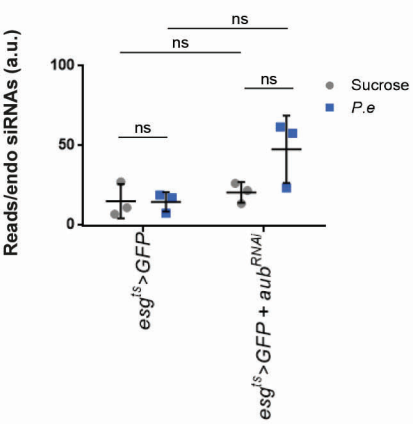

F

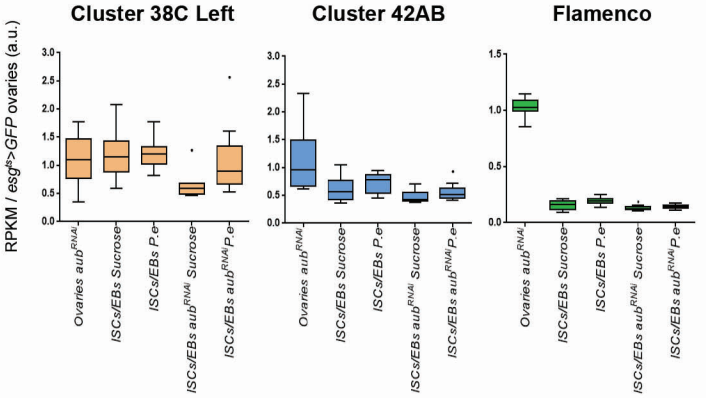

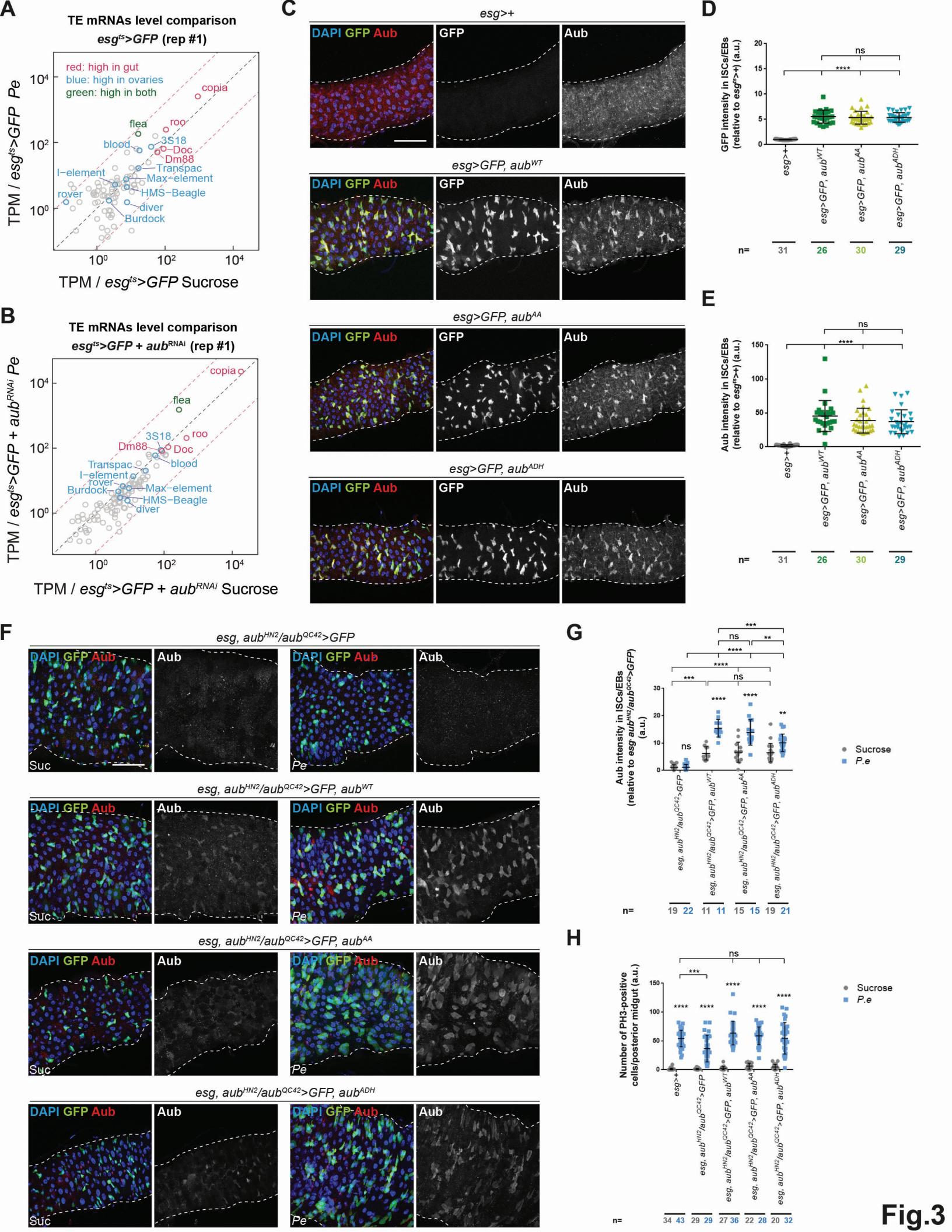
A
TE mRNAs level comparison
esg^ts>GFP (rep #1)
red: high in gut
blue: high in ovaries
green: high in both
copia
flea
roo
3S18
blood
Doc
Dm88
Transpac
I-element
Max-element
HMS-Beagle
rover
diver
Burdock
TPM / esg^ts>GFP Pe
TPM / esg^ts>GFP Sucrose
B
TE mRNAs level comparison
esg^ts>GFP + aub^RNAi (rep #1)
TPM / esg^ts>GFP + aub^RNAi Pe
TPM / esg^ts>GFP + aub^RNAi Sucrose
C
esg>+
esg>GFP, aub^WT
esg>GFP, aub^AA
esg>GFP, aub^ADH
DAPI GFP Aub
GFP
Aub
D
GFP intensity in ISCs/EBs (relative to esg^ts>+) (a.u.)
ns
****
esg>+
esg>GFP, aub^WT
esg>GFP, aub^AA
esg>GFP, aub^ADH
n= 31 26 30 29
E
Aub intensity in ISCs/EBs (relative to esg^ts>+) (a.u.)
F
esg, aub^HN2/aub^QC42>GFP
esg, aub^HN2/aub^QC42>GFP, aub^WT
esg, aub^HN2/aub^QC42>GFP, aub^AA
esg, aub^HN2/aub^QC42>GFP, aub^ADH
Suc
Pe
G
Aub intensity in ISCs/EBs (relative to esg aub^HN2/aub^QC42>GFP) (a.u.)
Sucrose
P.e
n= 19 22 11 11 15 15 19 21
H
Number of PH3-positive cells/posterior midgut (a.u.)
n= 34 43 29 29 27 36 22 28 20 32

Fig.3

Fig.4

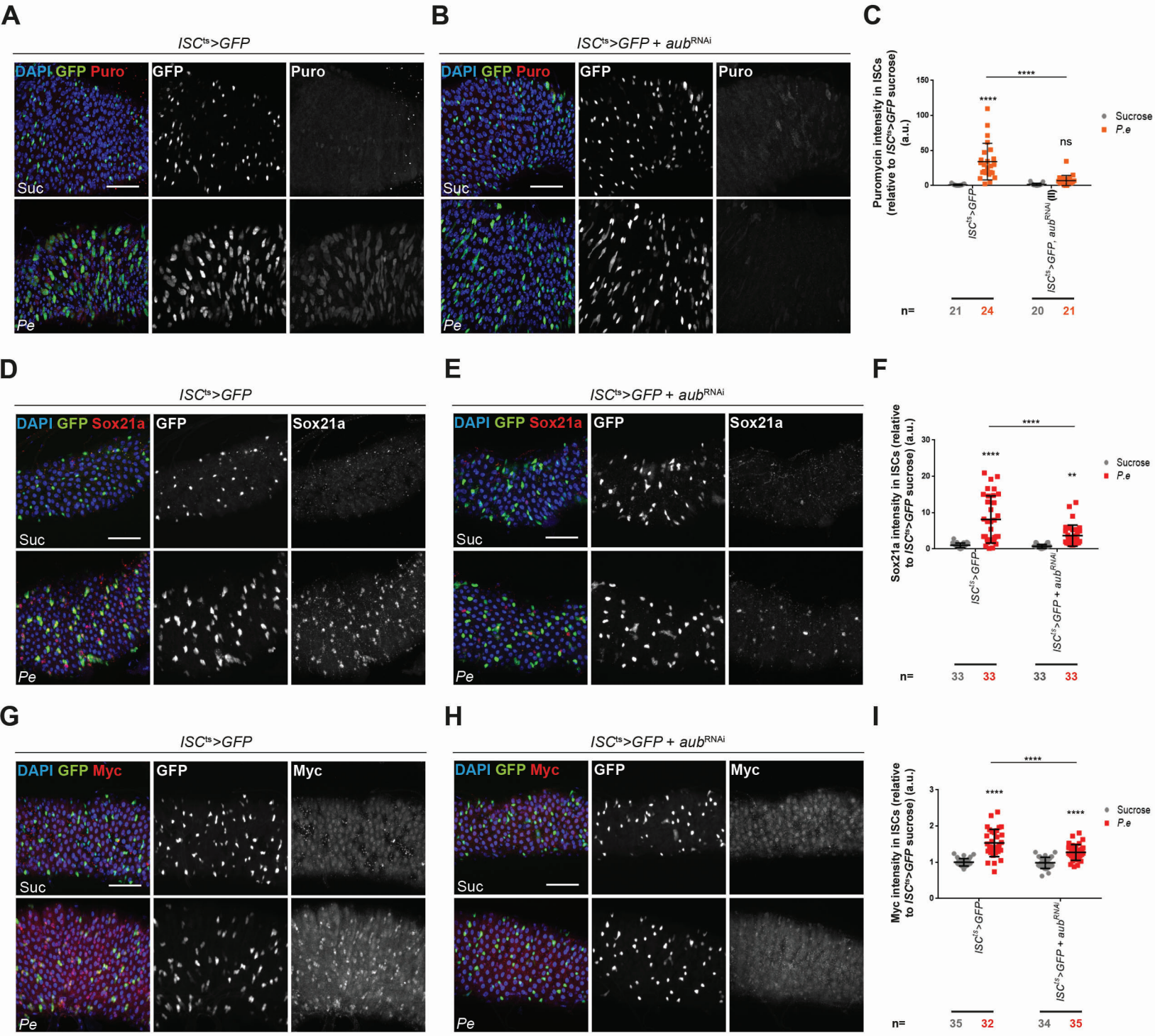
A
ISCts>GFP
DAPI GFP Puro
GFP
Puro
Suc
Pe
B
ISCts>GFP + aubRNAi
DAPI GFP Puro
GFP
Puro
Suc
Pe
C
Puromycin intensity in ISCs (relative to ISCts>GFP sucrose) (a.u.)
150
100
50
0
****
****
ns
Sucrose
P.e
ISCts>GFP
ISCts>GFP, aubRNAi (II)
n=
21
24
20
21
D
ISCts>GFP
DAPI GFP Sox21a
GFP
Sox21a
Suc
Pe
E
ISCts>GFP + aubRNAi
DAPI GFP Sox21a
GFP
Sox21a
Suc
Pe
F
Sox21a intensity in ISCs (relative to ISCts>GFP sucrose) (a.u.)
30
20
10
0
****
****
**
Sucrose
P.e
ISCts>GFP
ISCts>GFP + aubRNAi
n=
33
33
33
33
G
ISCts>GFP
DAPI GFP Myc
GFP
Myc
Suc
Pe
H
ISCts>GFP + aubRNAi
DAPI GFP Myc
GFP
Myc
Suc
Pe
I
Myc intensity in ISCs (relative to ISCts>GFP sucrose) (a.u.)
3
2
1
0
****
****
****
Sucrose
P.e
ISCts>GFP
ISCts>GFP + aubRNAi
n=
35
32
34
35

Fig.5

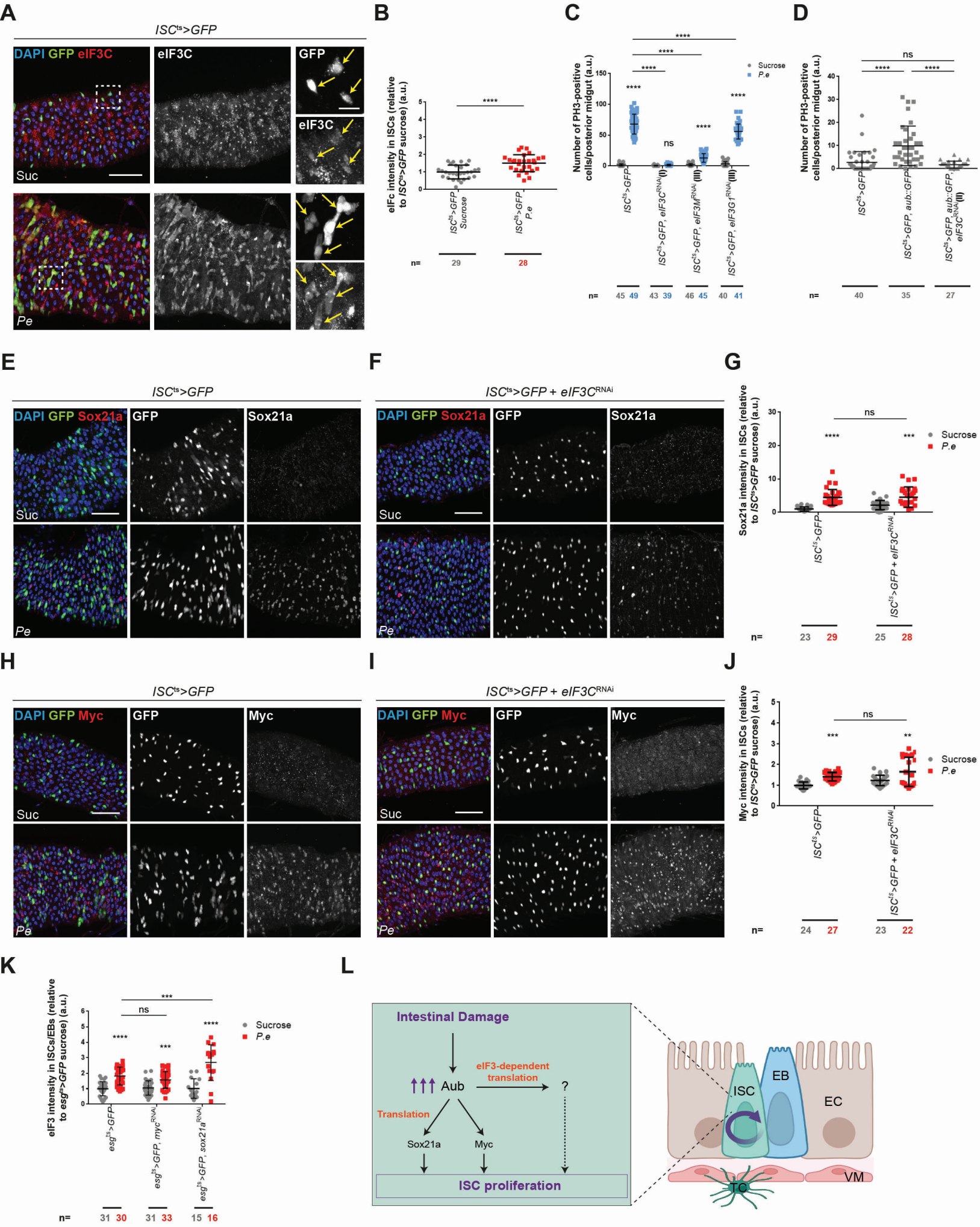
A
ISCts>GFP
DAPI GFP eIF3C
eIF3C
GFP
eIF3C
Suc
Pe
B
eIFc intensity in ISCs (relative to ISCts>GFP sucrose) (a.u.)
ISCts>GFP Sucrose
ISCts>GFP P.e
n= 29 28
C
Number of PH3-positive cells/posterior midgut (a.u.)
Sucrose
P.e
ISCts>GFP
ISCts>GFP, eIF3CRNAi (I)
ISCts>GFP, eIF3MRNAi (II)
ISCts>GFP, eIF3GRNAi (III)
n= 45 49 43 39 46 45 40 41
D
Number of PH3-positive cells/posterior midgut (a.u.)
ISCts>GFP
ISCts>GFP, aub::GFP
ISCts>GFP, aub::GFP, eIF3CRNAi (II)
n= 40 35 27
E
ISCts>GFP
DAPI GFP Sox21a
GFP
Sox21a
Suc
Pe
F
ISCts>GFP + eIF3CRNAi
DAPI GFP Sox21a
GFP
Sox21a
Suc
Pe
G
Sox21a intensity in ISCs (relative to ISCts>GFP sucrose) (a.u.)
Sucrose
P.e
ISCts>GFP
ISCts>GFP + eIF3CRNAi
n= 23 29 25 28
H
ISCts>GFP
DAPI GFP Myc
GFP
Myc
Suc
Pe
I
ISCts>GFP + eIF3CRNAi
DAPI GFP Myc
GFP
Myc
Suc
Pe
J
Myc intensity in ISCs (relative to ISCts>GFP sucrose) (a.u.)
Sucrose
P.e
ISCts>GFP
ISCts>GFP + eIF3CRNAi
n= 24 27 23 22
K
eIF3 intensity in ISCs/EBs (relative to esgts>GFP sucrose) (a.u.)
Sucrose
P.e
esgts>GFP
esgts>GFP, mycRNAi
esgts>GFP, sox21aRNAi
n= 31 30 31 33 15 16
L
Intestinal Damage
Aub
eIF3-dependent translation
?
Translation
Sox21a
Myc
ISC proliferation
ISC
EB
EC
TC
VM

Fig.6

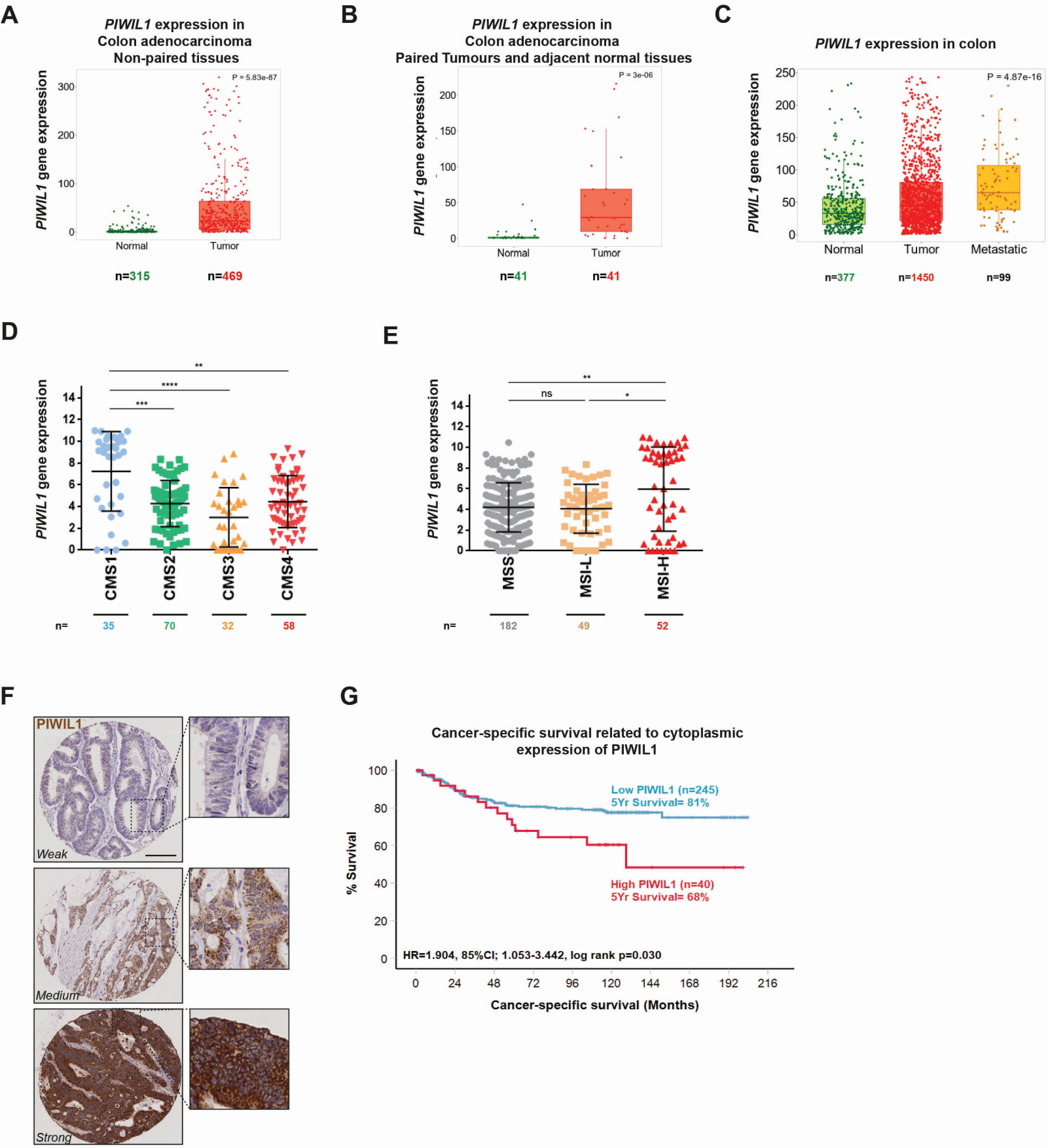
A
PIWIL1 expression in
Colon adenocarcinoma
Non-paired tissues
PIWIL1 gene expression
P = 5.83e-87
Normal
Tumor
n=315
n=469
B
PIWIL1 expression in
Colon adenocarcinoma
Paired Tumours and adjacent normal tissues
PIWIL1 gene expression
P = 3e-06
Normal
Tumor
n=41
n=41
C
PIWIL1 expression in colon
PIWIL1 gene expression
P = 4.87e-16
Normal
Tumor
Metastatic
n=377
n=1450
n=99
D
PIWIL1 gene expression
CMS1
CMS2
CMS3
CMS4
n=
35
70
32
58
E
PIWIL1 gene expression
MSS
MSI-L
MSI-H
n=
182
49
52
F
PIWIL1
Weak
Medium
Strong
G
Cancer-specific survival related to cytoplasmic
expression of PIWIL1
% Survival
Low PIWIL1 (n=245)
5Yr Survival= 81%
High PIWIL1 (n=40)
5Yr Survival= 68%
HR=1.904, 85%CI; 1.053-3.442, log rank p=0.030
Cancer-specific survival (Months)

Fig.7

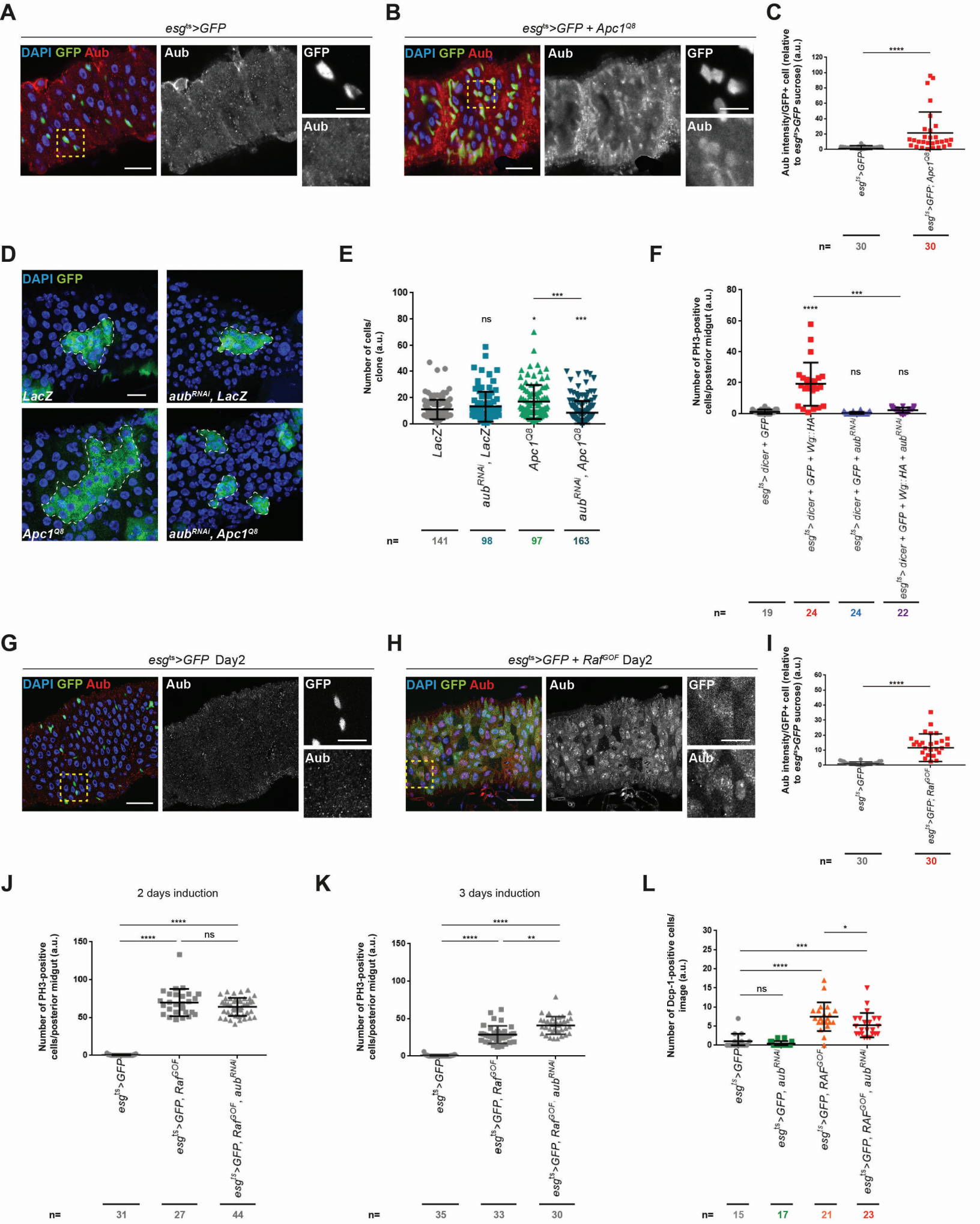
A
esg^ts>GFP
DAPI GFP Aub
Aub
GFP
Aub
B
esg^ts>GFP + Apc1^Q8
DAPI GFP Aub
Aub
GFP
Aub
C
Aub intensity/GFP+ cell (relative to esg^ts>GFP sucrose) (a.u.)
****
esg^ts>GFP
esg^ts>GFP; Apc1^Q8
n= 30 30
D
DAPI GFP
LacZ
aub^RNAi, LacZ
Apc1^Q8
aub^RNAi, Apc1^Q8
E
Number of cells/ clone (a.u.)
ns
*
***
***
LacZ
aub^RNAi, LacZ
Apc1^Q8
aub^RNAi, Apc1^Q8
n= 141 98 97 163
F
Number of PH3-positive cells/posterior midgut (a.u.)
****
***
ns
ns
esg^ts> dicer + GFP
esg^ts> dicer + GFP + Wg::HA
esg^ts> dicer + GFP + aub^RNAi
esg^ts> dicer + GFP + Wg::HA + aub^RNAi
n= 19 24 24 22
G
esg^ts>GFP Day2
DAPI GFP Aub
Aub
GFP
Aub
H
esg^ts>GFP + Raf^GOF Day2
DAPI GFP Aub
Aub
GFP
Aub
I
Aub intensity/GFP+ cell (relative to esg^ts>GFP sucrose) (a.u.)
****
esg^ts>GFP
esg^ts>GFP; Raf^GOF
n= 30 30
J
2 days induction
Number of PH3-positive cells/posterior midgut (a.u.)
****
****
ns
esg^ts>GFP
esg^ts>GFP, Raf^GOF
esg^ts>GFP, Raf^GOF, aub^RNAi
n= 31 27 44
K
3 days induction
Number of PH3-positive cells/posterior midgut (a.u.)
****
****
**
esg^ts>GFP
esg^ts>GFP, Raf^GOF
esg^ts>GFP, Raf^GOF, aub^RNAi
n= 35 33 30
L
Number of Dcp-1-positive cells/ image (a.u.)
*
***
****
ns
esg^ts>GFP
esg^ts>GFP, aub^RNAi
esg^ts>GFP, RAF^GOF
esg^ts>GFP, RAF^GOF, aub^RNAi
n= 15 17 21 23

Fig.S1

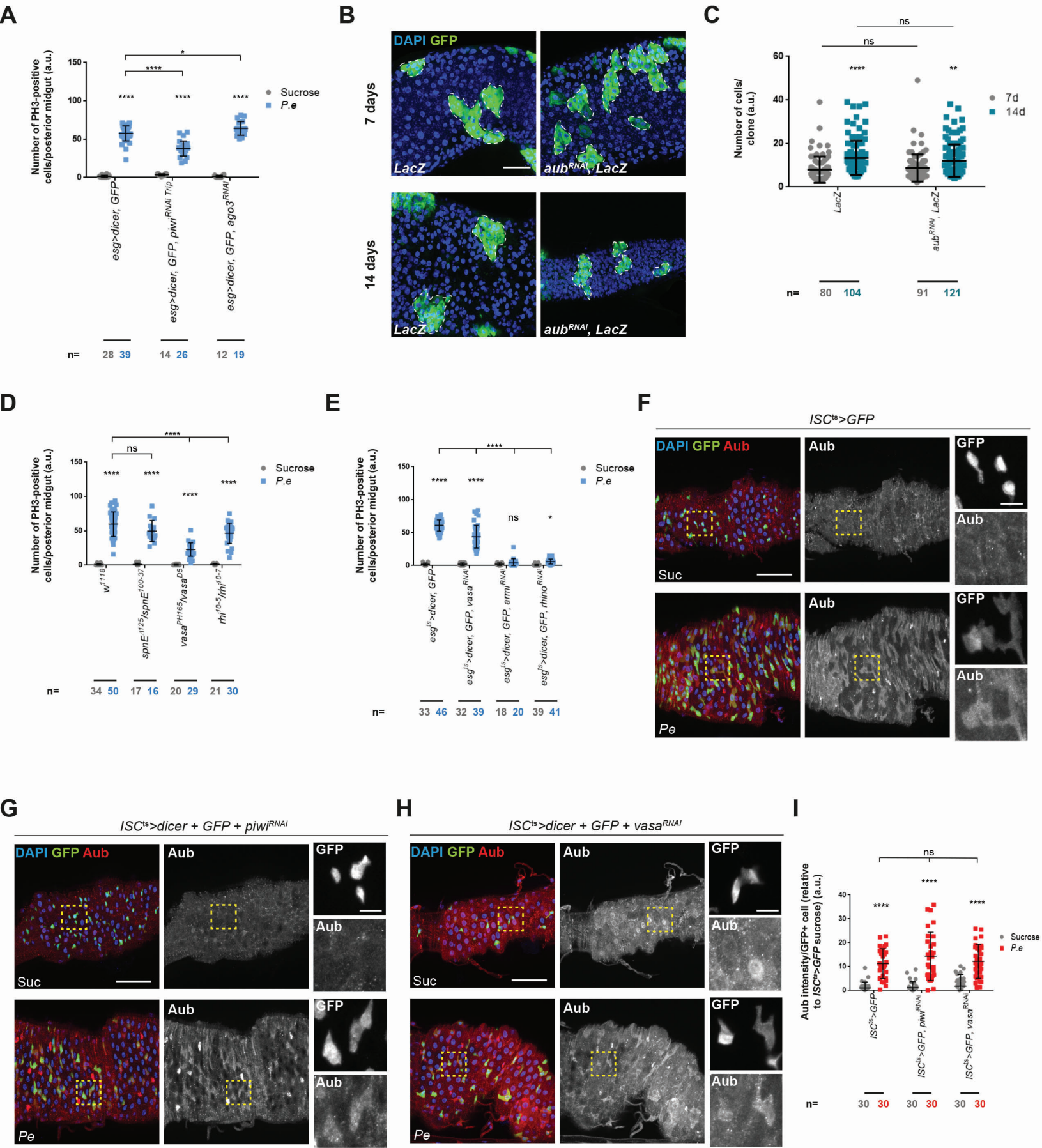
A
Number of PH3-positive cells/posterior midgut (a.u.)
Sucrose
P.e
esg>dicer, GFP
esg>dicer, GFP, piwi^RNAi Trip
esg>dicer, GFP, ago3^RNAi
n= 28 39 14 26 12 19
B
DAPI GFP
7 days
14 days
LacZ
aub^RNAi, LacZ
C
Number of cells/ clone (a.u.)
7d
14d
LacZ
aub^RNAi, LacZ
n= 80 104 91 121
D
Number of PH3-positive cells/posterior midgut (a.u.)
w^1118
spnE^1125/spnE^100-37
vasa^PH165/vasa^D5
rhi^18-5/rhi^18-7
n= 34 50 17 16 20 29 21 30
E
Number of PH3-positive cells/posterior midgut (a.u.)
esg^ts>dicer, GFP
esg^ts>dicer, GFP, vasa^RNAi
esg^ts>dicer, GFP, armi^RNAi
esg^ts>dicer, GFP, rhino^RNAi
n= 33 46 32 39 18 20 39 41
F
ISC^ts>GFP
DAPI GFP Aub
Aub
GFP
Suc
Pe
G
ISC^ts>dicer + GFP + piwi^RNAi
H
ISC^ts>dicer + GFP + vasa^RNAi
I
Aub intensity/GFP+ cell (relative to ISC^ts>GFP sucrose) (a.u.)
ISC^ts>GFP
ISC^ts>GFP, piwi^RNAi
ISC^ts>GFP, vasa^RNAi
n= 30 30 30 30 30 30

Fig.S2

A

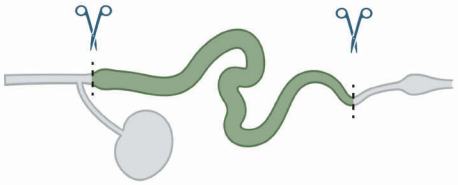

B

Oxidized library (rep #3)
w[1118] Sucrose

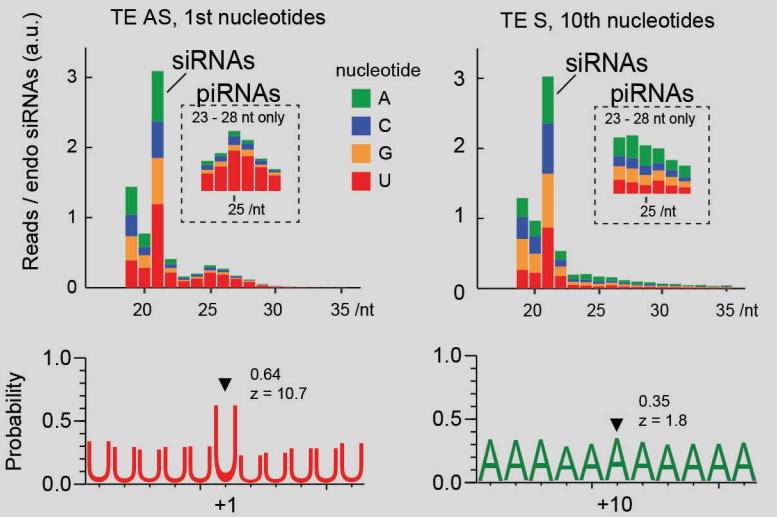

B'

Oxidized library (rep #2)
w[1118] *Pe*

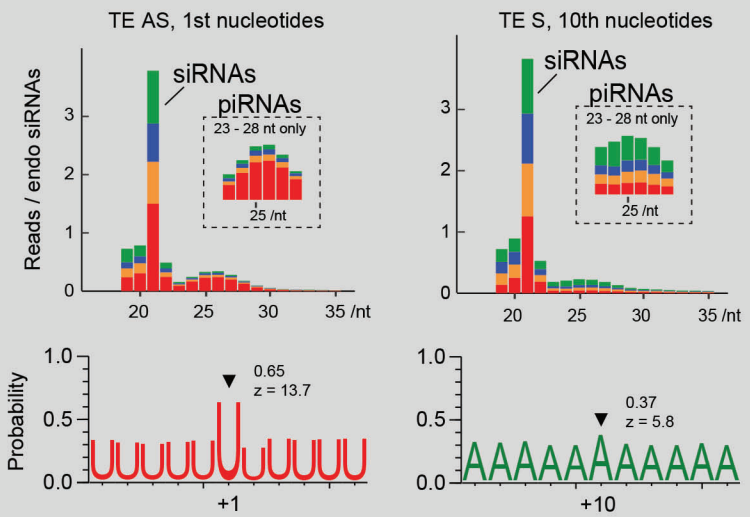

C

Oxidized library (rep #2)
aub Sucrose

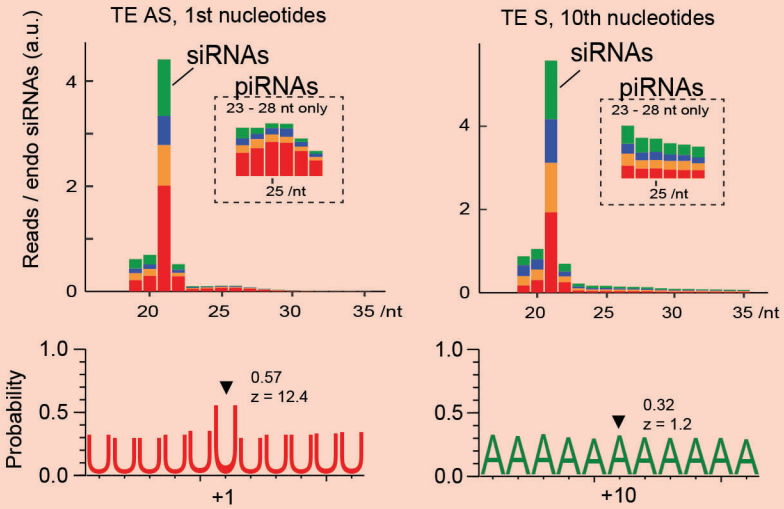

C'

Oxidized library (rep #3)
aub Pe

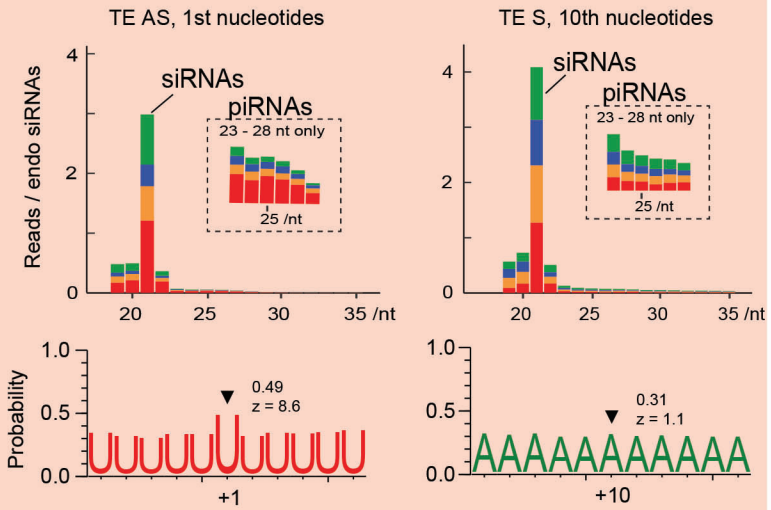

D

piRNAs Antisense

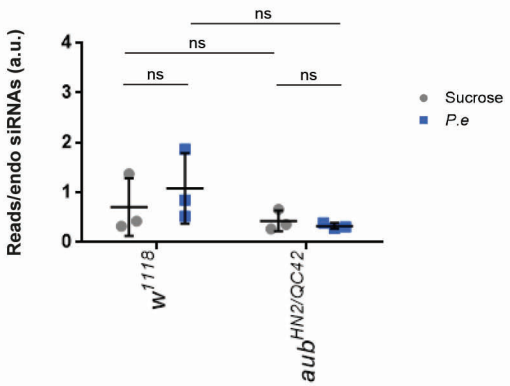

E

piRNAs Sense

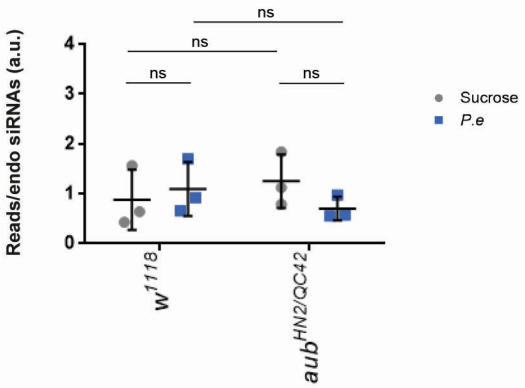

Fig.S3

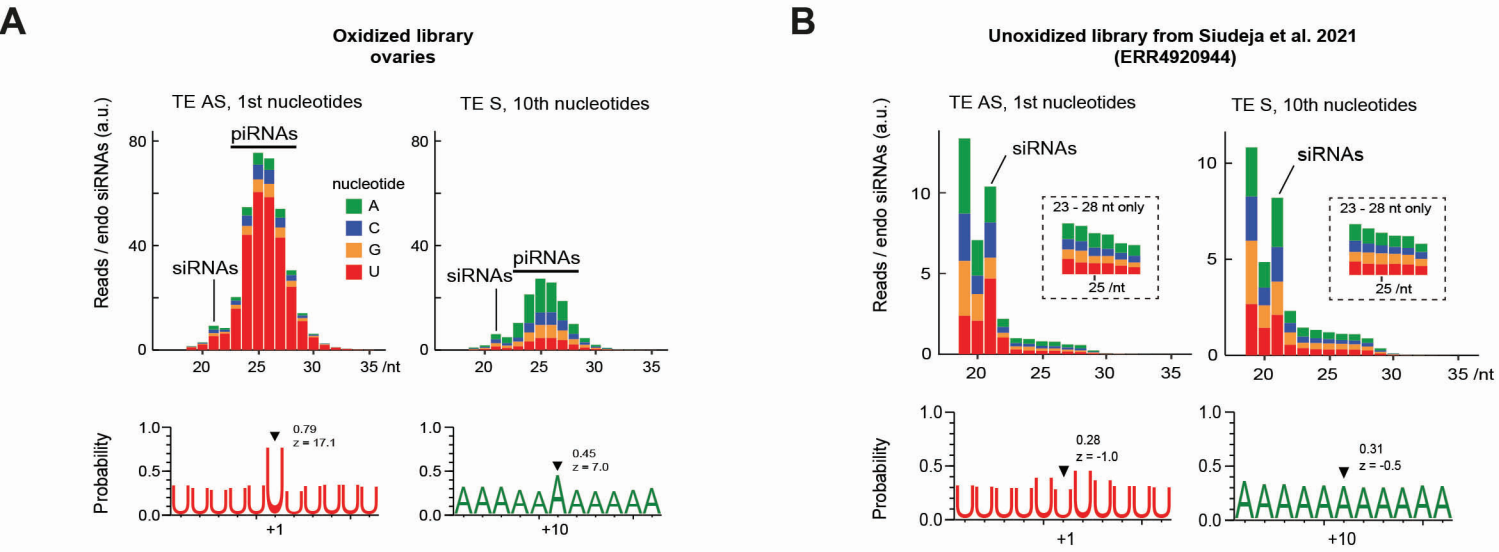
A
Oxidized library
ovaries
TE AS, 1st nucleotides
TE S, 10th nucleotides
Reads / endo siRNAs (a.u.)
piRNAs
siRNAs
nucleotide
A
C
G
U
35 /nt
Probability
0.79
z = 17.1
0.45
z = 7.0
+1
+10
B
Unoxidized library from Siudeja et al. 2021
(ERR4920944)
23 - 28 nt only
25 /nt
0.28
z = -1.0
0.31
z = -0.5

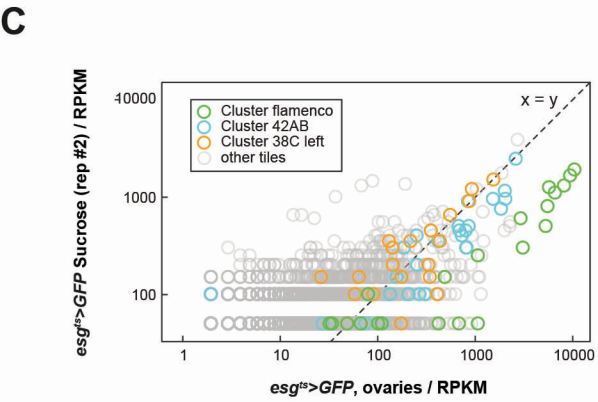
C
Cluster flamenco
Cluster 42AB
Cluster 38C left
other tiles
x = y
esg^ts>GFP Sucrose (rep #2) / RPKM
esg^ts>GFP, ovaries / RPKM

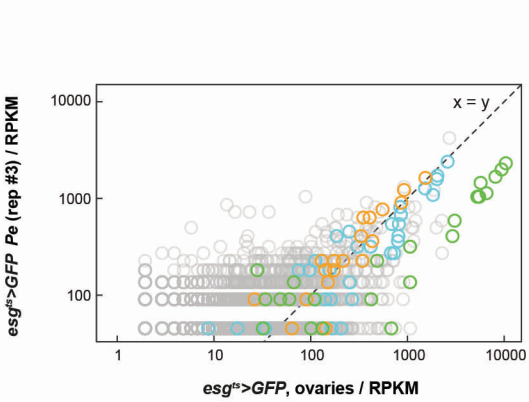
D
x = y
esg^ts>GFP Pe (rep #3) / RPKM
esg^ts>GFP, ovaries / RPKM

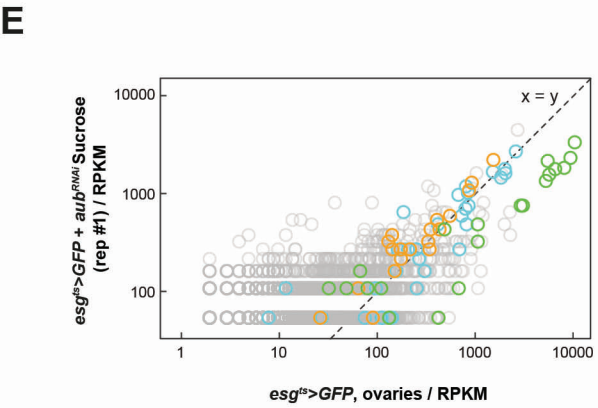
E
x = y
esg^ts>GFP + aub^RNAi Sucrose
(rep #1) / RPKM
esg^ts>GFP, ovaries / RPKM

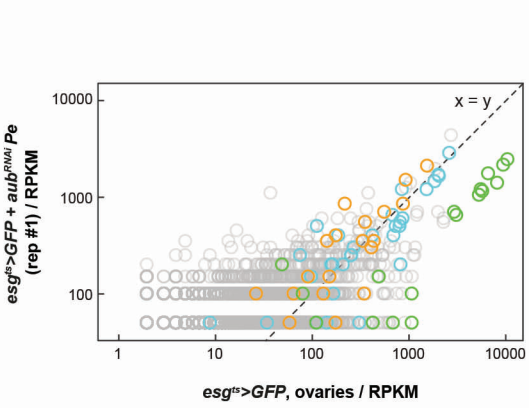
F
x = y
esg^ts>GFP + aub^RNAi Pe
(rep #1) / RPKM
esg^ts>GFP, ovaries / RPKM

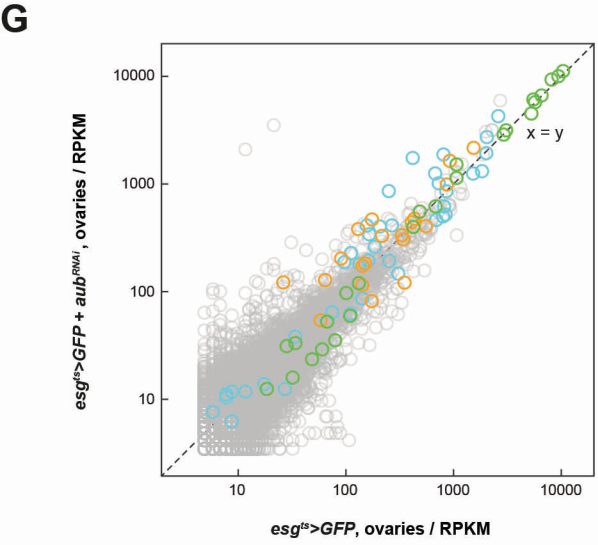
G
x = y
esg^ts>GFP + aub^RNAi, ovaries / RPKM
esg^ts>GFP, ovaries / RPKM

Fig.S4

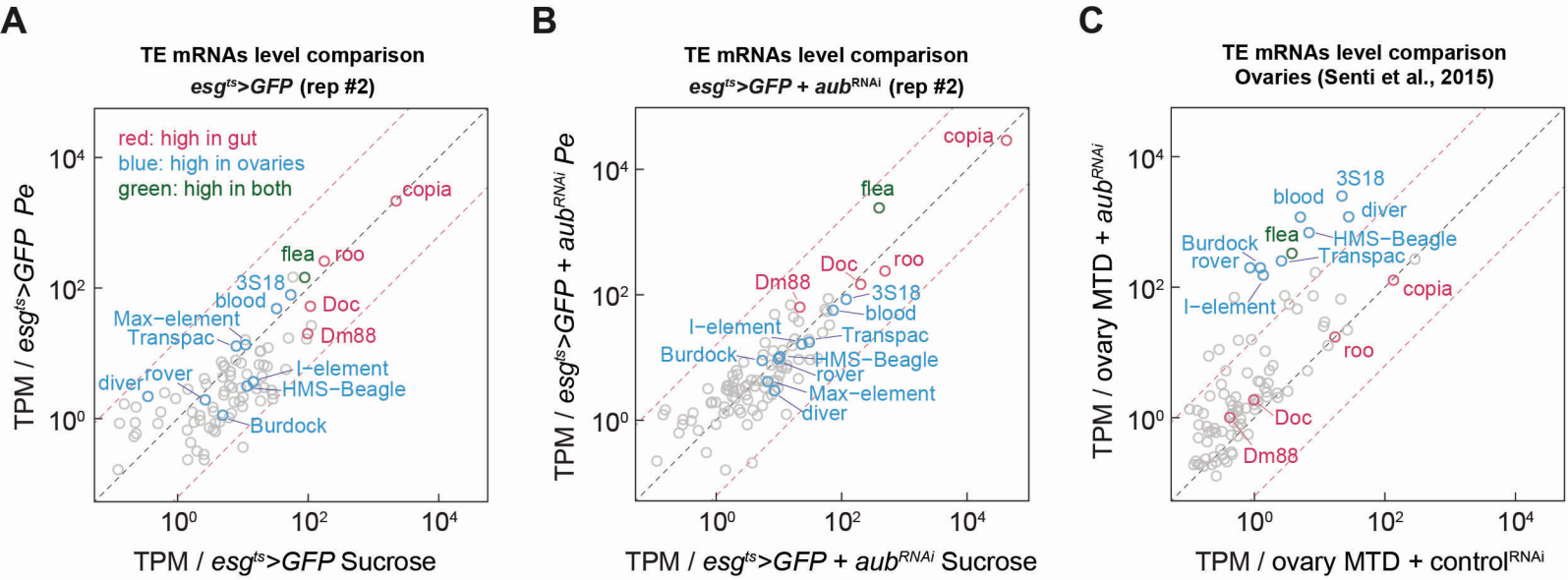

D

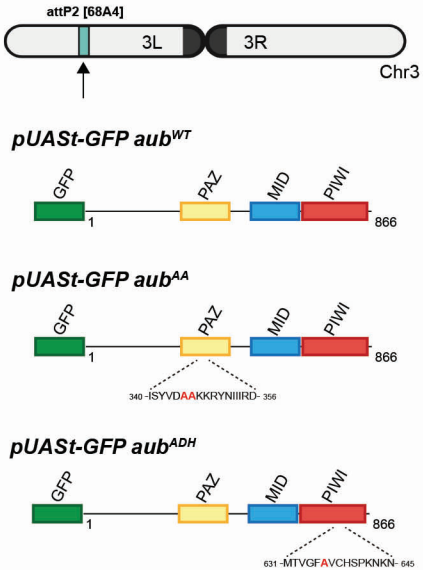

E

Maternal genotype	Average eggs per female per day	Egg laying rate (% compared to control)
aub ^{HN2}/*aub* ^{QC42}, *nos*>+	0.004166667	0.05
aub ^{HN2}/*aub* ^{QC42}, *nos*>*aub* ^{WT}	1.6125	19.53
aub ^{HN2}/*aub* ^{QC42}, *nos*>*aub* ^{AA}	0.047222222	0.6
aub ^{HN2}/*aub* ^{QC42}, *nos*>*aub* ^{ADH}	0.0125	0.15

Fig.S5

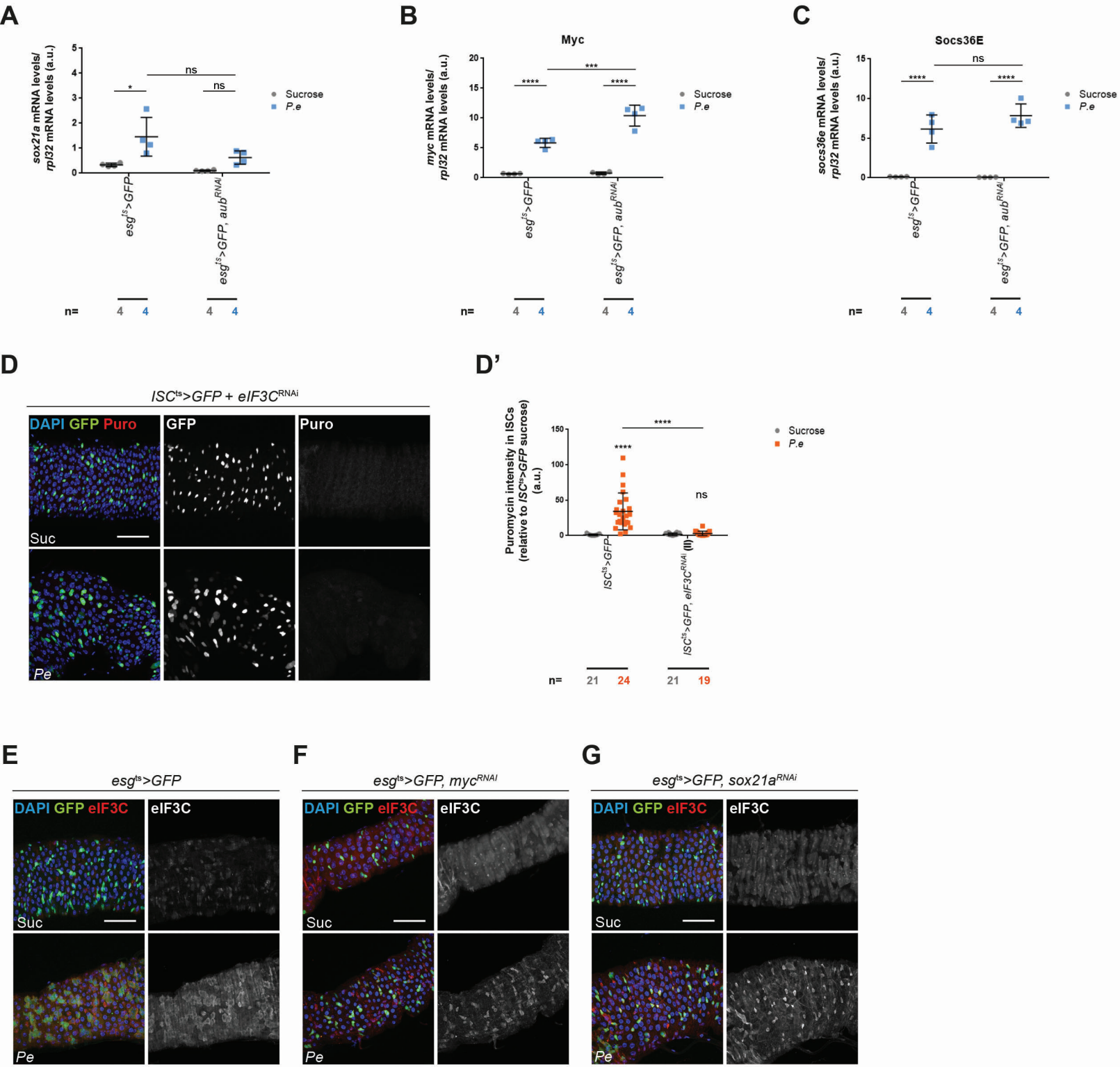
A
sox21a mRNA levels/ rpl32 mRNA levels (a.u.)
ns
*
ns
Sucrose
P.e
esg^ts>GFP
esg^ts>GFP, aub^RNAi
n= 4 4 4 4
B
Myc
myc mRNA levels/ rpl32 mRNA levels (a.u.)
***
****
****
Sucrose
P.e
esg^ts>GFP
esg^ts>GFP, aub^RNAi
n= 4 4 4 4
C
Socs36E
socs36e mRNA levels/ rpl32 mRNA levels (a.u.)
ns
****
****
Sucrose
P.e
esg^ts>GFP
esg^ts>GFP, aub^RNAi
n= 4 4 4 4
D
ISC^ts>GFP + eIF3C^RNAi
DAPI GFP Puro
GFP
Puro
Suc
Pe
D'
Puromycin intensity in ISCs (relative to ISC^ts>GFP sucrose) (a.u.)
****
****
ns
Sucrose
P.e
ISC^ts>GFP
ISC^ts>GFP, eIF3C^RNAi (II)
n= 21 24 21 19
E
esg^ts>GFP
DAPI GFP eIF3C
eIF3C
Suc
Pe
F
esg^ts>GFP, myc^RNAi
DAPI GFP eIF3C
eIF3C
Suc
Pe
G
esg^ts>GFP, sox21a^RNAi
DAPI GFP eIF3C
eIF3C
Suc
Pe

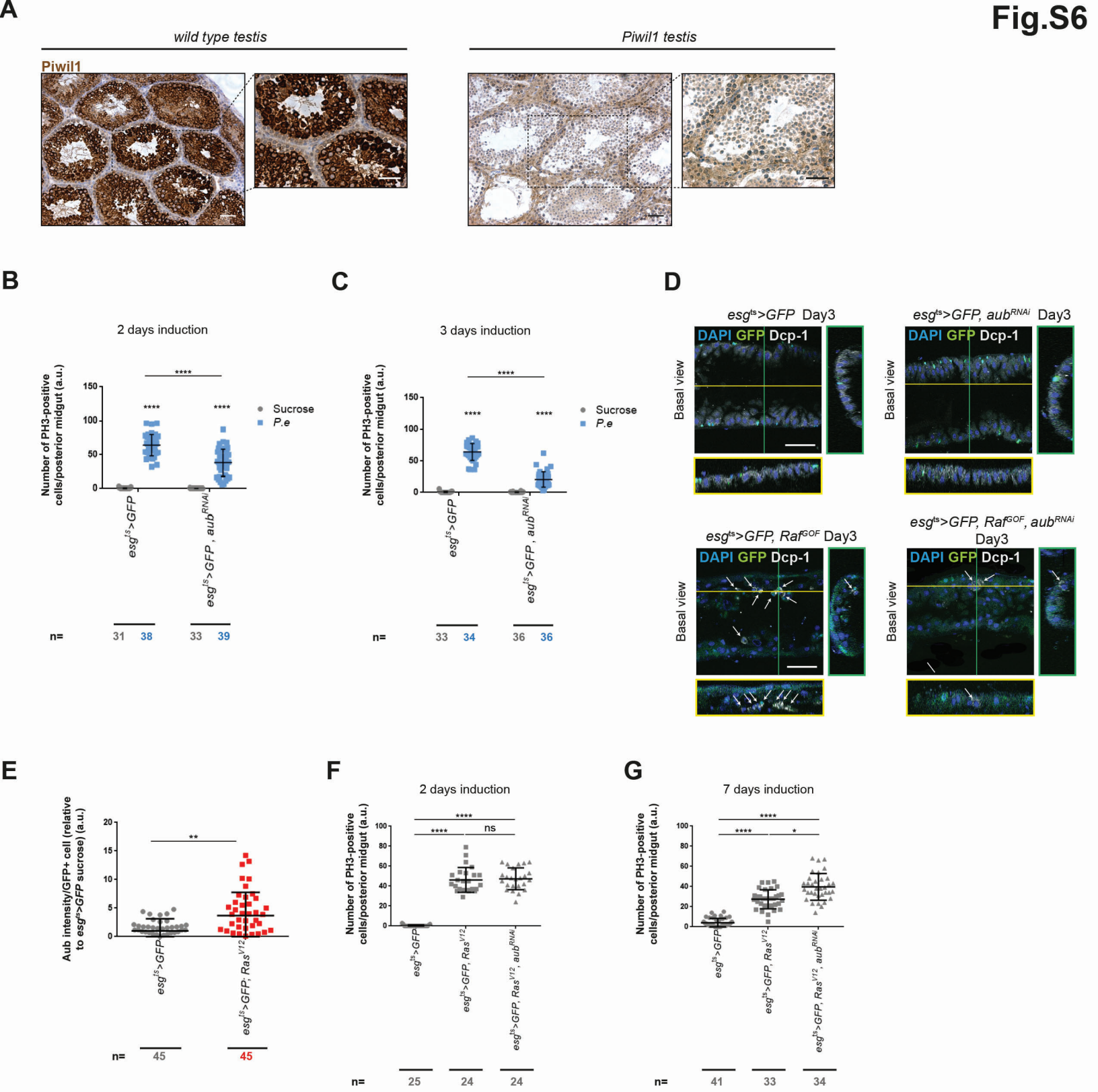

Fig.S6
A
wild type testis
Piwil1 testis
Piwil1
B
2 days induction
Number of PH3-positive cells/posterior midgut (a.u.)
Sucrose
P.e
esg^ts>GFP
esg^ts>GFP , aub^RNAi
n=
31
38
33
39
C
3 days induction
Number of PH3-positive cells/posterior midgut (a.u.)
Sucrose
P.e
esg^ts>GFP
esg^ts>GFP , aub^RNAi
n=
33
34
36
36
D
esg^ts>GFP Day3
esg^ts>GFP, aub^RNAi Day3
esg^ts>GFP, Raf^GOF Day3
esg^ts>GFP, Raf^GOF, aub^RNAi Day3
DAPI GFP Dcp-1
Basal view
E
Aub intensity/GFP+ cell (relative to esg^ts>GFP sucrose) (a.u.)
esg^ts>GFP
esg^ts>GFP; Ras^V12
n=
45
45
F
2 days induction
Number of PH3-positive cells/posterior midgut (a.u.)
ns
esg^ts>GFP
esg^ts>GFP, Ras^V12
esg^ts>GFP, Ras^V12, aub^RNAi
n=
25
24
24
G
7 days induction
Number of PH3-positive cells/posterior midgut (a.u.)
esg^ts>GFP
esg^ts>GFP, Ras^V12
esg^ts>GFP, Ras^V12, aub^RNAi
n=
41
33
34